

SPITZER'S CONTRIBUTION TO THE AGN POPULATION

J. L. DONLEY,¹ G. H. RIEKE,¹ P. G. PÉREZ-GONZÁLEZ,^{2,3} G. BARRO²

Accepted for publication in the Astrophysical Journal; 2008 June 26

ABSTRACT

Infrared selection is a potentially powerful way to identify heavily obscured AGN missed in even the deepest X-ray surveys. Using a 24 μ m-selected sample in GOODS-S, we test the reliability and completeness of three infrared AGN selection methods: (1) IRAC color-color selection, (2) IRAC power-law selection, and (3) IR-excess selection; we also evaluate a number of infrared excess approaches. We find that the vast majority of non-power-law IRAC color-selected AGN candidates in GOODS-S have colors consistent with those of star-forming galaxies. Contamination by star-forming galaxies is most prevalent at low 24 μ m flux densities ($\sim 100 \mu$ Jy) and high redshifts ($z \sim 2$), but the fraction of potential contaminants is still high ($\sim 50\%$) at 500 μ Jy, the highest flux density probed reliably by our survey. AGN candidates selected via a simple, physically-motivated power-law criterion (PLGs), however, appear to be reliable. We confirm that the infrared excess methods successfully identify a number of AGN, but we also find that such samples may be significantly contaminated by star-forming galaxies. Adding only the secure *Spitzer*-selected PLG, color-selected, IR-excess, and radio/IR-selected AGN candidates to the deepest X-ray-selected AGN samples directly increases the number of known X-ray AGN (84) by 54 – 77%, and implies an increase to the number of 24 μ m-detected AGN of 71 – 94%. Finally, we show that the fraction of MIR sources dominated by an AGN decreases with decreasing MIR flux density, but only down to $f_{24 \mu\text{m}} = 300 \mu$ Jy. Below this limit, the AGN fraction levels out, indicating that a non-negligible fraction ($\sim 10\%$) of faint 24 μ m sources (the majority of which are missed in the X-ray) are powered not by star formation, but by the central engine. The fraction of all AGN (regardless of their MIR properties) exceeds 15% at all 24 μ m flux densities.

Subject headings: galaxies: active — infrared: galaxies — X-rays: galaxies

1. INTRODUCTION

Identifying complete and reliable samples of AGN has become a necessity for extragalactic surveys, whether the goal be the selection of AGN candidates or the removal of AGN “contaminants”. Only when armed with complete samples of AGN will we be able to determine the role of obscured accretion in the build-up of the present day black hole mass function, or accurately characterize the star-formation history of the universe. Complete AGN samples are also required to test proposed evolutionary theories in which black hole formation and star-formation are intimately linked by merger and feedback processes (e.g. Hopkins et al. 2006), ultimately producing the correlation between black hole mass and bulge velocity dispersion (Ferrarese & Merritt 2000; Gebhardt et al. 2000). Unfortunately, the varied luminosities, accretion rates, orientations, and intrinsic obscurations of AGN prevent any one selection technique from reliably identifying all of them. For instance, while current UV, optical, and X-ray surveys are capable of detecting unobscured AGN, they miss many of the obscured AGN and nearly all of the Compton-thick AGN thought to dominate AGN number counts at both low and high redshift (e.g. Gilli et al. 2007; Daddi et al. 2007a,b). Likewise, only 10-15% of AGN are radio-loud, making radio

surveys relatively incomplete.

The Multiband Imaging Photometer (MIPS; Rieke et al. 2004) and Infrared Array Camera (IRAC; Fazio et al. 2004) instruments aboard *Spitzer* have provided sensitive surveys in multiple mid-IR bands. Infrared selection with MIPS and IRAC data is being used widely to select AGN candidates independently of their optical and/or X-ray properties. In addition to identifying AGN in fields with little or no X-ray data, infrared selection criteria are capable of identifying heavily obscured AGN missed in even the deepest X-ray fields (e.g. Donley et al. 2007). As such, IR selection has the potential to complement traditional AGN selection methods and to yield a more complete census of AGN activity.

In this paper, we critically review the following infrared selection criteria: (1) IRAC color-color selection, (2) IRAC power-law selection, and (3) IR-excess selection. The first selection method employs color cuts in two representations of IRAC 4-band mid-infrared (MIR) color-color space (Lacy et al. 2004; Stern et al. 2005), the second identifies AGN whose IRAC SEDs are well-fit by a power-law (Alonso-Herrero et al. 2006; Donley et al. 2007), and the third selects red galaxies with large infrared to UV/optical flux ratios (Daddi et al. 2007a; Dey et al. 2008; Fiore et al. 2008; Polletta et al. 2008). The first two criteria are based on the same principle: the hot dust near an AGN's central engine reprocesses absorbed UV, optical, and X-ray emission into short-wavelength MIR emission, filling in the gap between the stellar emission that peaks near 1.5 μ m and the long-wavelength dust emission features that dominate the SEDs of star-forming

¹ Steward Observatory, University of Arizona, 933 North Cherry Avenue, Tucson, AZ 85721; jdonley@as.arizona.edu

² Departamento de Astrofísica y CC. de la Atmósfera, Facultad de CC. Físicas, Universidad Complutense de Madrid, 28040 Madrid, Spain

³ Associate Astronomer at Steward Observatory, The University of Arizona

galaxies. The color-color and power-law selection criteria, however, differ in the range of mid-IR characteristics they include as possible AGN indicators. The third selection method identifies sources in which heavy obscuration with reemission in the infrared diminishes the optical emission and/or enhances the infrared emission.

This paper utilizes improved spectral templates with a sample of infrared color-selected, power-law galaxies (PLGs), and IR-excess galaxies in the ultra-deep GOODS-S field to test the reliability and completeness of these selection techniques over a wide range of sample properties. From this analysis, we then quantify the contribution of these approaches plus *Spitzer* identification of radio-intermediate and radio-loud AGN to the X-ray-selected AGN population. The paper is organized as follows. In §2, we describe the selection of the color-selected, PLG, and IR-excess samples. The construction of high-reliability photometric redshifts is described in §3, as are the overall redshift properties of the sample. In §4, we briefly discuss the X-ray properties of our MIPS-selected sample. The infrared color selection criteria of Lacy et al. (2004) and Stern et al. (2005) are discussed in §5, where we compare and contrast the two selection criteria, investigate the behavior in color space of the star-forming templates, determine the redshift and flux dependencies of the color selection techniques, and investigate the properties of the most secure color-selected AGN candidates. In §6, we discuss the PLG selection criteria, and in §7 we investigate the IR-excess sources. Finally, in §8, we discuss the overall statistics of AGN revealed by IR-based methods compared with X-ray-selected samples. A summary is given in §9. Throughout the paper, we assume the following cosmology: $(\Omega_m, \Omega_\Lambda, H_0) = (0.3, 0.7, 72 \text{ km s}^{-1} \text{ Mpc}^{-1})$.

2. SAMPLE SELECTION

2.1. Multi-wavelength Data

We take as our initial GOODS-S sample all MIPS sources detected at $24 \mu\text{m}$ to a flux density of $f_{24 \mu\text{m}} > 80.0 \mu\text{Jy}$. At this flux limit, 99% of the MIPS sample are detected to $> 10\sigma$. There are several advantages to choosing a flux-limited MIPS sample. First, AGN (and LIRGS/ULIRGS) tend to be bright at $24 \mu\text{m}$ (e.g. Rigby et al. 2004). Selecting only those galaxies with $f_{24 \mu\text{m}} > 80.0 \mu\text{Jy}$ therefore retains all but the faintest AGN while excluding 50-60% of IRAC-selected IR-normal star-forming galaxies at all flux densities. Second, a MIPS flux-limited sample is not subject to the complicated slope-dependent selection bias present in IRAC selected samples due to the significant variation in the sensitivity of the 4 IRAC bands (see Donley et al. 2007). Third, this selection gives a complete and well-defined sample of objects with extreme red $R - [24]$ colors.

The MIPS $24 \mu\text{m}$ catalog of the GOODS Legacy team (Dickinson et al., in prep.) is comprised of 948 sources in the MIPS CDF-S Legacy field with $f_\nu > 80.0 \mu\text{Jy}$. While this MIPS depth can be obtained over the full CDF-S, we chose to limit this study to the GOODS region to take advantage of the super-deep IRAC imaging. The relative depths of the limiting MIPS flux and the super-deep IRAC photometry ensure that essentially all MIPS sources have high S/N IRAC SEDs, allowing us to study

in an unbiased way the IRAC properties of this flux-limited MIPS sample. To ensure that all AGN candidates have sufficient X-ray coverage, we also required X-ray coverage of $T_X > 250 \text{ ks}$ from the deep 1 Ms CDF-S X-ray dataset (see Giacconi et al. (2002) and Alexander et al. (2003)). Despite this relatively low cut, 96% of the final MIPS sample have $T_X > 0.5 \text{ Ms}$ and 80% have $T_X > 0.75 \text{ Ms}$. The resulting sample was drawn from an area of 195.3 sq. arcmin and contains 846 MIPS sources.

The CDF-S is one of the best-imaged fields in the UV, optical, NIR, and X-ray. We took advantage of this extensive multiwavelength dataset by creating an aperture-matched catalog using the UV-NIR photometry of Marzke et al. (1999, *RIz*), Vandame et al. (2001, *JK*), Arnouts et al. (2002, *UU_pBVRI*), COMBO17 (Wolf et al. 2004), Giavalisco et al. (2004, *bvzJHK*), Le Fèvre et al. (2004, *I*), and GALEX (*FUV, NUV*) (see Pérez-González et al. 2005 and the UCM Extragalactic Database⁴ for more details). We then removed from our sample the 89 MIPS sources that had multiple optical counterparts that were (1) within a $2.5''$ search radius of the MIPS source and (2) separated by more than $0.5''$. (At $r < 0.5''$, it is difficult to distinguish between multiple counterparts and an extended/irregular source with multiple components.) While we do not restrict our sample to regions covered by GOODS ACS imaging, 83% of the MIPS sources in our sample have deep ACS coverage.

SExtractor-selected IRAC sources were similarly matched to the MIPS sample after combining the super-deep IRAC data with data from the deep, wide-area, *Spitzer* Legacy Program (PI: van Dokkum) and the MIPS-GTO IRAC program (see Pérez-González et al. 2008 for further details). To ensure accurate MIR SEDs, we removed from the IR PLG and color-selected samples 32 sources with blended IRAC or MIPS photometry. Of the remaining 725 MIPS sources that meet our criteria, 713 (98%) have unique IRAC counterparts within a $2''$ search radius, and 699 (96%) have $> 5\sigma$ IRAC detections in all 4 IRAC bands, allowing us to determine accurately the MIR colors of essentially all members of the MIPS-selected sample. Of the 12 sources without IRAC counterparts, 6 were not detected due to blending with a nearby source, 4 had badly centered MIPS positions, and 2 had faint IRAC counterparts that fall below our catalog limit.

2.2. Power-law, color-selected, and IR-normal samples

After assigning IRAC counterparts, we separated the MIPS sample into three subsets: IR PLGs, IR color-selected galaxies, and IR-normal galaxies. We defined as PLGs sources whose 4-band IRAC photometry is well-fit by a line of slope $\alpha \leq -0.5$, where $f_\nu \propto \nu^\alpha$ (Alonso-Herrero et al. 2006; Donley et al. 2007). The effect of different cuts in α will be discussed in §6. To ensure a good fit, we required the chi-squared probability P_χ (the probability that the fit would yield a chi-squared greater than or equal to the observed chi-squared) to exceed 0.1. P_χ tends either to lie close to 0.5 (the probability that corresponds to a reduced chi-squared of 1) or is very small (see Bevington & Robinson 2003). This selection, which identified 55 PLGs, was done using the LINFIT task in

⁴ <http://t-rex.fis.ucm.es/pgperez/Proyectos/databaseuse.en.html>

IDL. This task takes the following 4-band input from IRAC:

$$x = \log(\nu) \quad (1)$$

$$y = \log(f_\nu) \quad (2)$$

$$\Delta y = [1/\ln(10)] * \Delta f_\nu / f_\nu \quad (3)$$

and returns the best fit slope, α , and the chi-squared probability, P_χ . While sources selected via this method are dominated by the AGN in the mid-IR, we do not require that the power-law extend into the optical. Consequently, many infrared-selected PLGs are dominated by stellar emission at wavelengths short of $\sim 2 \mu\text{m}$, where the reprocessed emission from hot dust is suppressed because of dust sublimation.

Color-selected galaxies were defined as sources that meet the AGN IRAC color-cuts of Lacy et al. (2004) or Stern et al. (2005), but that **do not meet the PLG criterion**. As discussed in Alonso-Herrero et al. (2006) and Donley et al. (2007), both the PLG and IRAC color cuts attempt to select luminous AGN that outshine their host galaxies in the infrared, filling in the dip in a galaxy's SED between the short-wavelength stellar emission feature and the long-wavelength dust emission features. As such, the IRAC AGN color selection regions contain, but also extend beyond, the power-law locus in color space. While nearly all PLGs meet the IRAC AGN color selection criteria, not all color-selected galaxies meet the PLG criteria. We therefore separate color-selected sources that can be identified via a power-law fit (PLGs) from those that can not (color-selected galaxies). The color-selected sample consists of 210 sources, 188 of which meet the Lacy et al. criteria, 72 of which meet the Stern et al. criteria, and 50 of which meet both criteria.

Finally, we define IR-normal galaxies as sources that meet neither the IRAC PLG nor the color selection criteria; these sources comprise the remaining 448 galaxies in the MIPS sample. As they are not the focus of this study, we have not checked their IRAC and MIPS photometry by eye. Instead, we estimate that the fraction of IR-normal galaxies with blended IRAC or MIPS photometry is similar to that found for the PLG and color-selected samples, 11%, or ~ 50 galaxies. We caution that IR-normal does *not* mean purely star-forming. Instead, 'IR-normal' only indicates that any mid-IR emission from an AGN is overwhelmed by emission from the host-galaxy. In fact, many Type 2 and Seyfert-luminosity AGN meet the IR-normal criteria (Stern et al. 2005, Donley et al. 2007, Cardamone et al. 2008).

2.3. IR-Excess Galaxies

In addition to dividing the MIPS-selected sample into the 3 sub-samples discussed above, we identified IR-excess galaxies using the criteria of Daddi et al. (2007a), Dey et al. (2008), Fiore et al. (2008), and Polletta et al. (2008). (We also searched for bright ULIRGS that met the IR-excess criteria of Yan et al. (2007), but found none in our faint sample.) Daddi et al. (2007a) selected galaxies in GOODS (with a 3σ $24 \mu\text{m}$ flux limit of $15\text{--}30 \mu\text{Jy}$) whose total MIR+UV star-formation rate (SFR) exceeds the dust-corrected UV SFR by a factor of > 3 , and estimate that at least $\sim 50\%$ of their sample are Compton-thick AGN. Dey et al. (2008) select

sources with $R - [24] \geq 14$ ($f_{24 \mu\text{m}}/f_R \gtrsim 1000$) and $f_{24 \mu\text{m}} > 300 \mu\text{Jy}$, criteria which yield a sample of both heavily obscured AGN and star-forming galaxies. Fiore et al. similarly require that $f_{24 \mu\text{m}}/f_R \geq 1000$, but also include an optical/NIR criterion of $R - K > 4.5$ and extend their selection to fainter $24 \mu\text{m}$ fluxes of $f_{24 \mu\text{m}} \geq 40 \mu\text{Jy}$. They estimate from simulations that 80% of the sources selected via these criteria are obscured AGN. Polletta et al. (2008) focus only on the most luminous AGN ($f_{24 \mu\text{m}} \gtrsim 1 \text{ mJy}$) with large infrared to optical flux ratios, whose IRAC and MIPS colors can be described by the following criteria: $f_{5.8}/f_{3.6} > 2$, $f_{8.0}/f_{4.5} > 2$, and $\log[f_{8.0}/f_{3.6}] + \log[f_{24}/f_{3.6}] > 2$.

Because IR-excess sources tend to be optically-faint, we use the approach of Fiore et al. (2008, private communication) and estimate the R-band magnitudes by interpolating the ACS v- and i-band data from the MUSIC catalog (Grazian et al. 2006). Despite the inherent uncertainties associated with this relatively simple method, the interpolated R-band magnitudes are in excellent agreement with ground-based R-band measurements for bright sources, and they greatly improve upon the uncertain R-band estimations at faint flux densities. Because the MUSIC catalog is based on identifications at z and K (the latter of which is universally bright for the IR-excess sources), the use of the MUSIC catalog for these sources also ensures that the correct optical counterpart is chosen, as verified by a visual inspection of the sources selected via the Fiore et al. criteria. The only disadvantage of this method is that, of the 195.3 sq. arcmin of our survey, only 132.7 sq. arcmin (68%) are covered by the deep ISAAC K-band data, which was also used in the selection of the Daddi et al. sources. Our identification of the Dey et al., Daddi et al., and Fiore et al. IR-excess samples is therefore limited to this region.

Of the 465/713 sources in our MIPS-selected sample that lie in the ISAAC field, 10 meet the Dey et al. criteria, 52 meet the Fiore et al. criteria, and 42 lie in the Daddi et al. IR-excess sample (the list of which was kindly provided by D. Alexander, private communication 2008). In addition, 71 MIPS sources have red IR/optical colors of $f_{24 \mu\text{m}}/f_R \geq 1000$; we will refer to this sample as 'IR-bright/optically-faint'. Of the full sample of 713 sources, 5 meet the Polletta et al. criteria. The properties of these IR-excess galaxies, nearly all of which also meet the power-law or color-selection criteria outlined above, will be discussed in more detail in §7.

3. REDSHIFTS

While the redshift coverage in the CDF-S is amongst the highest in all cosmological fields, only 34% of the sources in our faint sample have spectroscopic redshifts. As one of our main goals is to investigate the redshift-dependency of infrared color selection, we require both accurate and complete redshift information. However, the mean magnitude of the sources without spectroscopic redshifts, $V \sim 24.1$, is very faint, making further spectroscopic follow-up challenging. We therefore supplement the spectroscopic redshifts with photometric ones. The sources that are the focus of this study generally have SEDs with weak stellar features and require extra care to fit accurate photometric redshifts. To insure this accuracy, we have used two complementary photo-z ap-

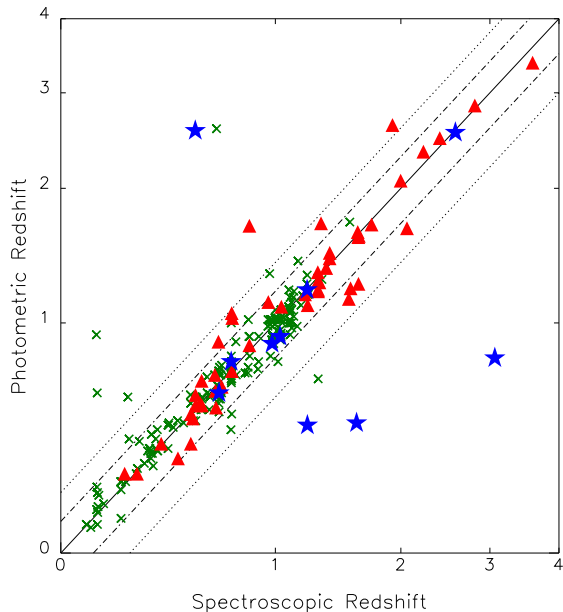


FIG. 1.— Photometric vs. secure spectroscopic redshifts for PLGs (navy stars), color-selected galaxies (red triangles), and IR-normal galaxies (green crosses). Values are plotted in $\log(1+z)$. Dot-dashed and dotted lines give 10% and 20% errors on Δz , respectively. 89% of the sample have $\Delta(z) < 0.1$, and 95% have $\Delta(z) < 0.2$.

proaches and have incorporated two stages of independent visual inspection by two reviewers, as described in Appendix A. The final results, shown in Figure 1, support the high accuracy and completeness of the adopted redshifts for this faint sample.

Of the 713 MIPS-selected sources in our sample, 249 have secure spectroscopic redshifts from the VVDS (Le Fèvre et al. 2004), VLT/FORS2 (Vanzella et al. 2006), K20 (Mignoli et al. 2005), and Szokoly et al. (2004) redshift surveys. For our photometric redshifts, the mean offset is $\overline{\Delta(z)} = 0.012$, where $\Delta(z) = (z_p - z_s)/(1 + z_s)$, and the dispersion is $\sigma_z = 0.15$, where $\sigma_z^2 = (1/N) \sum \Delta(z)^2$. Eighty-nine percent of the sample have $\Delta(z) < 0.1$, and 95% have $\Delta(z) < 0.2$. As shown in Table 1, while the redshift completeness and accuracy are high for the IR-normal and color-selected samples, they drop significantly for the PLG sample. A comparison of their spectroscopic and photometric redshifts illustrates some of the issues. Three of the four PLG outliers are best fit by a Type 1 QSO template, whose redshift is particularly difficult to constrain. However, of the 18 PLGs for which only photometric redshifts are available, only 2 (11%) are fit by a Type 1 QSO template. The remainder show optical features/breaks that make their redshift determination more secure. As such, we expect the overall accuracy of the PLG redshifts to be higher than one would assume given the limited comparison with spectroscopic redshifts.

With the addition of 400 photometric redshifts, computed as described above, our redshift completeness is 91%. The redshift distribution is shown in Figure 2. Also plotted in Figure 2 is a redshift histogram that incorporates typical errors in the photometric redshifts. To produce this distribution, we simulated 10,000 redshift distributions in which the photometric redshifts were randomly varied according to the appropriate σ given in Table 1. We plot in Figure 2 the mean of the resulting

distributions. Both redshift distributions show a strong peak at $z = 1$, and while the first shows a potential peak at $z \sim 2$, we cannot confirm its presence due to the errors on the photometric redshifts.

We separate the sample in Figure 2 into the PLG, color-selected (Lacy et al. and Stern et al.), and IR-normal subsamples. As expected, the number of IR-normal galaxies peaks at $z = 0.7$ (a well-known redshift peak in the CDF-S) and at $z = 1.1$ (another known redshift peak). We also detect a peak at $z = 0.3$ similar to that found by Desai et al. (2008), whose strength increases if we apply their cut of $f_{24} \mu\text{m} \geq 300 \mu\text{Jy}$. In the CDF-S, however, this peak is dwarfed by the stronger peak at $z = 0.7$, even at large flux densities. The redshift distribution of the IR-normal galaxies decreases rapidly at redshifts of $z > 1.2$, where only highly luminous star-forming galaxies are detectable. In contrast, the PLGs with redshift estimates have a relatively flat distribution in redshift space, as was found for the PLGs in the CDF-N (Donley et al. 2007).

The redshift distributions of the (non-power-law) Lacy et al. and Stern et al. selected samples differ significantly, both from the IR-normal and PLG samples, as well as from one another. The Stern-selected galaxies peak at $z \sim 1.25$ whereas the Lacy-selected galaxies show significant peaks at $z \sim 0.5$ and $z \sim 2$, with very few galaxies falling in the $z < 1$ regime originally probed by these selection methods (see §5). In addition, at $z \geq 1.75$, nearly all (94%) MIPS-selected sources meet the Lacy AGN selection criteria, regardless of their nature. A large concentration of galaxies at $z \sim 2$ was previously observed in this field by Caputi et al. (2006), and in a brighter sample of MIPS sources by Desai et al. (2008), and is most probably due to the $7.7 \mu\text{m}$ aromatic feature passing through the $24 \mu\text{m}$ band. This behavior suggests that the mid-IR continua of the Lacy color-selected galaxies contain substantial contributions from star-formation (e.g. Genzel et al. 1998).

Finally, the mean redshifts of the IR-excess samples are as follows: $z = 1.92 \pm 0.36$ for the Daddi et al. sources, $z = 2.19 \pm 0.61$ for the dust obscured galaxies (DOGs, Dey et al. 2008), $z = 2.09 \pm 0.48$ for the Fiore-selected sources, $z = 2.11$ for the one Polletta source with a known redshift, and $z = 2.05 \pm 0.49$ for the IR-bright/optically-faint sources. As discussed above, this concentration about a redshift of 2 (when not a design of the selection as in Daddi et al. (2007)) is likely to be due at least in part to the passage of the $7.7 \mu\text{m}$ aromatic feature through the MIPS $24 \mu\text{m}$ band, suggesting a significant contribution from star-formation.

4. X-RAY PROPERTIES

Of the 713 MIPS sources, 109 (15%) have X-ray counterparts in the Alexander et al. (2003) or Giacconi et al. (2002) catalogs. Of these, 25 are PLGs, 35 are color-selected galaxies (33 from the Lacy criteria, and 12 from the Stern criteria), and 49 are IR-normal. While the IR-normal galaxies therefore dominate the X-ray counts, the fraction of such sources is low: only 11% of the IR-normal galaxies have X-ray counterparts, as compared to 17% of the color-selected galaxies and 45% of the PLGs.

We test for faint ($\geq 2\sigma$) X-ray emission from the MIPS sources using the procedure outlined in Donley et al. (2005). The resulting detection fractions for the

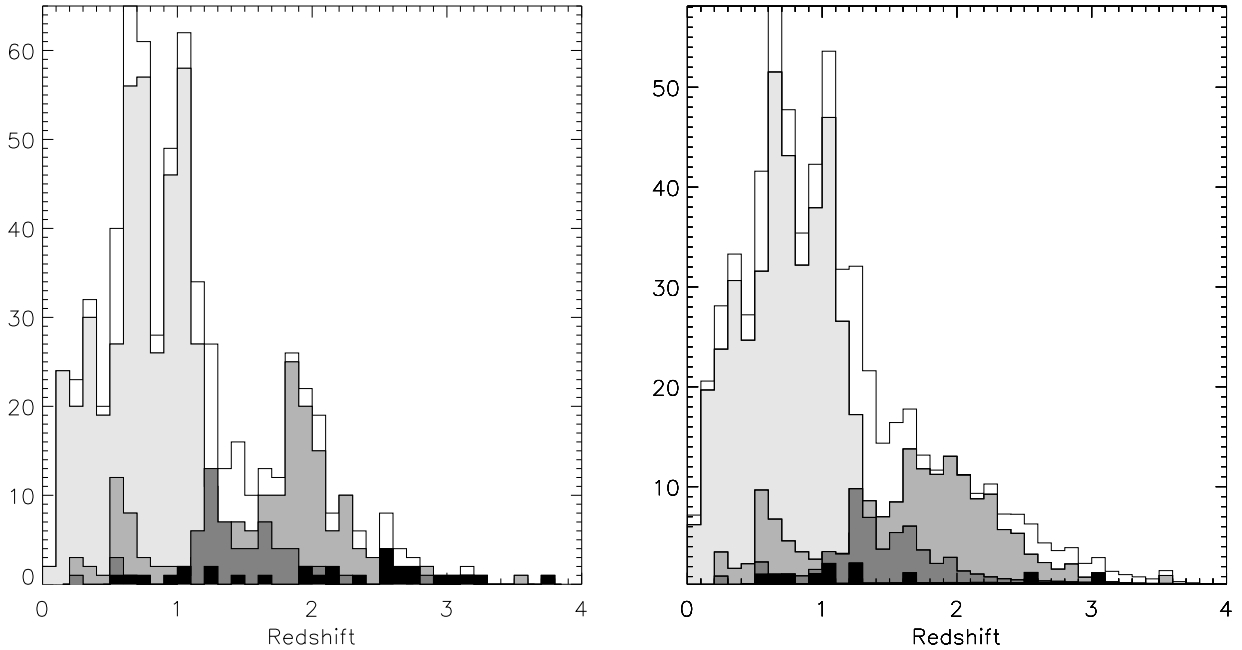


FIG. 2.— Redshift distribution of the MIPS-selected sample. The plot on the left gives the observed distribution, while the plot on the right incorporates the typical errors on the photometric redshifts. From lightest to darkest shading, the histograms represent all MIPS sources in our sample, IR-normal galaxies, color-selected sources that meet the Lacy et al. (2004) criteria, color-selected sources that meet the Stern et al. (2005) criteria, and PLGs.

PLG, color-selected, IR-normal, and IR-excess samples are given in Table 2. With the inclusion of the weakly-detected X-ray sources, the detection fractions of the IR-normal, color-selected, and PLG samples increase to 40%, 42%, and 64%, respectively. As indicated in Table 2, however, while all strongly and weakly-detected PLGs have AGN X-ray luminosities of $\log L_x(\text{ergs s}^{-1}) \geq 42$, the same is true for only 74% of the color-selected galaxies, and 34% of the IR-normal galaxies. Given the infrared luminosities implied by our $24 \mu\text{m}$ selection criterion, the portion of the sample with $\log L_x(\text{ergs s}^{-1}) < 42$ will be heavily contaminated with star-forming galaxies (Ranalli et al. 2003).

While the X-ray detection fraction of PLGs is relatively low (though significantly higher than that of the color-selected galaxies), it is comparable to that of previously-selected samples (Alonso-Herrero et al. 2006, Donley et al. 2007). Of the PLGs in the 2 Ms CDF-N, 55% had high-significance X-ray counterparts. However, only 15% remained undetected down to the 2.5σ detection level, suggesting that many PLGs are likely to be heavily obscured X-ray sources whose fluxes fall below the current detection limits (Donley et al. 2007). In the CDF-S, only 45% of the PLGs have cataloged X-ray counterparts and 36% remain undetected down to 2σ . This slightly lower detection fraction is due at least in part to the lower X-ray exposure of the 1 Ms CDF-S, and will be discussed further in §6.

The X-ray detection fraction of the luminous IR-excess sources selected via the Polletta et al. (2008) sample is high (80%). However, the same can not be said for the remaining IR-excess samples: only 30% of the DOGs, 19% of the Fiore et al. sources, and 15% of the sources with high $24 \mu\text{m}$ to optical flux ratios have cataloged X-ray counterparts. By definition, none of the Daddi et al. sources have cataloged hard X-ray counterparts, although 3 have soft-band counterparts. When the weakly-

detected X-ray counterparts are included, these numbers rise to 100% for the Polletta sources, 63% for the DOGs, 44% for the Daddi et al. sources, 43% for the Fiore et al. sources, and 42% for the IR-bright/optically-faint sources.

5. IRAC COLOR-COLOR SELECTION

There are several reasons why a re-examination of the color-color selection criteria is needed before applying these techniques to our sample. First, thanks to the availability of high quality NIR and *Spitzer* MIR spectra and photometry, we can now construct more accurate MIR templates for both AGN and star-forming galaxies than were available when the Lacy et al. and Stern et al. AGN selection criteria were initially defined. Second, the AGN selection criteria of Lacy and Stern were initially designed for use with shallow surveys, and have not yet been properly tested over a range of both redshift and flux density (but see Cardamone et al. 2008). Third, photometric redshift techniques for *Spitzer*-detected galaxies have advanced sufficiently to allow nearly complete redshift estimation.

The positions of the MIPS-selected sample in IRAC color space are shown in Figure 3, where stars represent the PLGs and circles represent the remaining MIPS sources. As expected, all PLGs meet the Lacy criteria and all but 3 meet the Stern criteria. The relatively large scatter of the PLGs on the Stern plot probably arises in part from the use of adjacent color bands, whereas the power-law fitting tends to smooth over noise.

5.1. Comparison of the IRAC color-color selection criteria

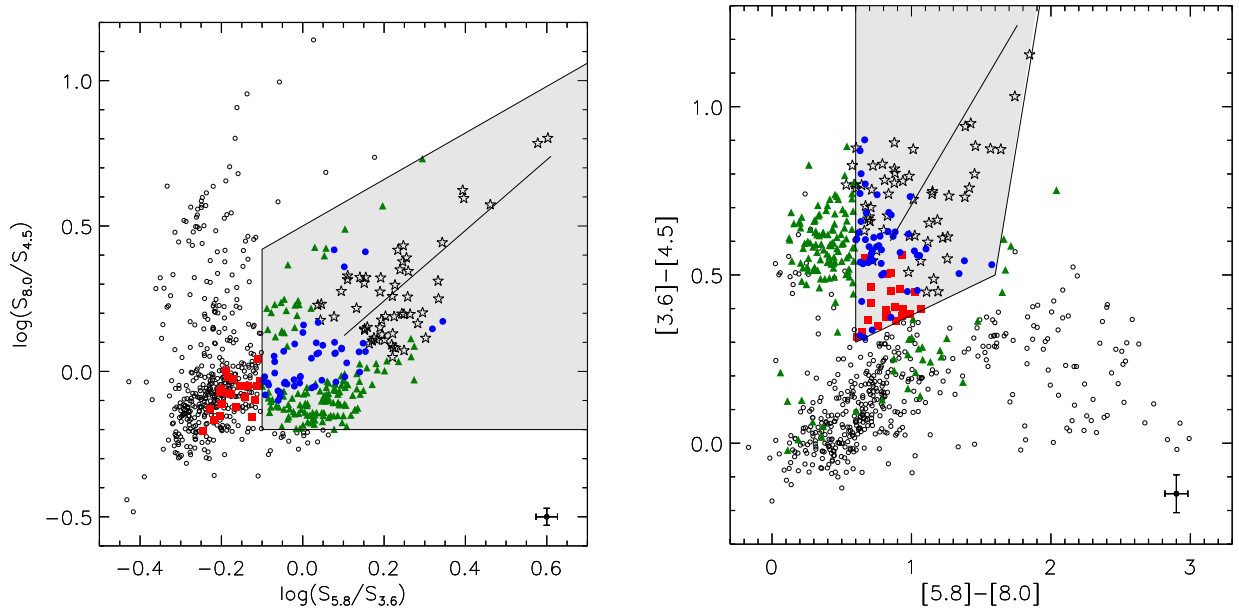


FIG. 3.— Position in Lacy et al. (2004; left) and Stern et al. (2005; right) color-space of the MIPS-selected sample, where PLGs are given as stars. Blue filled circles represent color-selected galaxies that meet both the Lacy et al. and Stern et al. criteria. Green triangles and red squares represent sources that meet only the Lacy et al. or Stern et al. criteria, respectively. The small open circles are IR-normal galaxies. The shaded regions represent the AGN selection regions, and the diagonal lines within are the loci of perfect power laws with $\alpha = -0.5$ to -3.0 .

To illuminate the strengths and weaknesses of the two color-color selection criteria in Figure 3, we separate the sources that meet both the Lacy et al. (2004) and Stern et al. (2005) AGN selection criteria from those that meet only one of the two criteria. The color-selected sources that meet both criteria primarily define an extension of the power-law locus to a blue slope of $\alpha = +0.5$ (recall that our definition of PLGs includes only those sources with red slopes of $\alpha < -0.5$). We will discuss in detail the effects of different power-law slope criteria in §6.

The Lacy-only sources occupy two regions in color-space. The first, located in the lower portion of the Lacy diagram, corresponds to the concentration in the upper-left corner of the Stern et al. selection region. These sources were intentionally excluded from the Stern selection region to minimize contamination from high-redshift ($z \sim 2$) star-forming galaxies. The second concentration of Lacy-only galaxies is scattered throughout the star-forming locus of the Stern diagram. Are these normal, low- z star-forming galaxies, or obscured AGN not selected by the Stern criteria?

The Stern-only sources fall almost exclusively in the lower left portion of the Stern wedge, and occupy the region dominated by low-redshift IR-normal galaxies in the Lacy et al. color diagram, suggesting that, like the Lacy criteria, the Stern et al. criteria are likely to suffer from low-redshift star-forming galaxy contamination. Because of the exclusion of $z \sim 2$ star-forming galaxies, however, the Stern et al. criteria should perform better at high z . To test this hypothesis, we next consider the evolution in IRAC color-space of a number of high-quality star-forming and AGN templates.

5.2. Star-forming Templates

As discussed above, the availability of high-quality near- and mid-infrared data has allowed the construction of high-quality star-forming SEDs, particularly for

luminous and ultra-luminous infrared galaxies (LIRGS and ULIRGS). In Figure 4, we plot the redshift evolution of these templates in IRAC color-color space over $z = 0 - 4$, where purple and blue tracks represent the *purely star-forming* ULIRG and LIRG templates of Rieke et al. (2008, see Table A1), green tracks represent the spiral and starburst templates of Polletta et al. (2007) and Dale & Helou (2002), and red tracks represent the elliptical templates of Silva et al. (1998). Large circles mark the tracks at $z = 0$, and small circles mark each integer redshift from $z = 1$ to 4.

While the star-forming templates generally avoid the power-law locus itself, they enter the Lacy and Stern selection regions at both low and high redshifts, tracing out the same regions in color space occupied by many of the color-selected AGN, particularly those selected via only one of the two criteria. The templates therefore suggest potential star-forming galaxy contamination of the color-selected AGN, as previously predicted by Barmby et al. (2006), Donley et al. (2007), and Cardamone et al. (2008), and indicate that the current AGN selection regions may inadequately separate AGN and star-forming galaxies.

Our results can be compared with the simulations of Sajina, Lacy, & Scott (2005), who calculated mathematical models of galaxies from three spectral components: stars, aromatic features, and a continuum. For $0 < z < 1$, we agree with their Figure 8 (upper left) that starburst luminosity galaxies do not significantly ‘invade’ the Lacy AGN color wedge (see our Figure 4). However, we find that more luminous galaxies can invade this wedge much more seriously (again see Figure 4). The difference may arise because the inputs to their models included few star-forming LIRGs and only one ULIRG (Arp 220, an atypical case). Therefore, it is likely that the behavior of the most luminous star forming galaxies is not captured as accurately in their models as is that

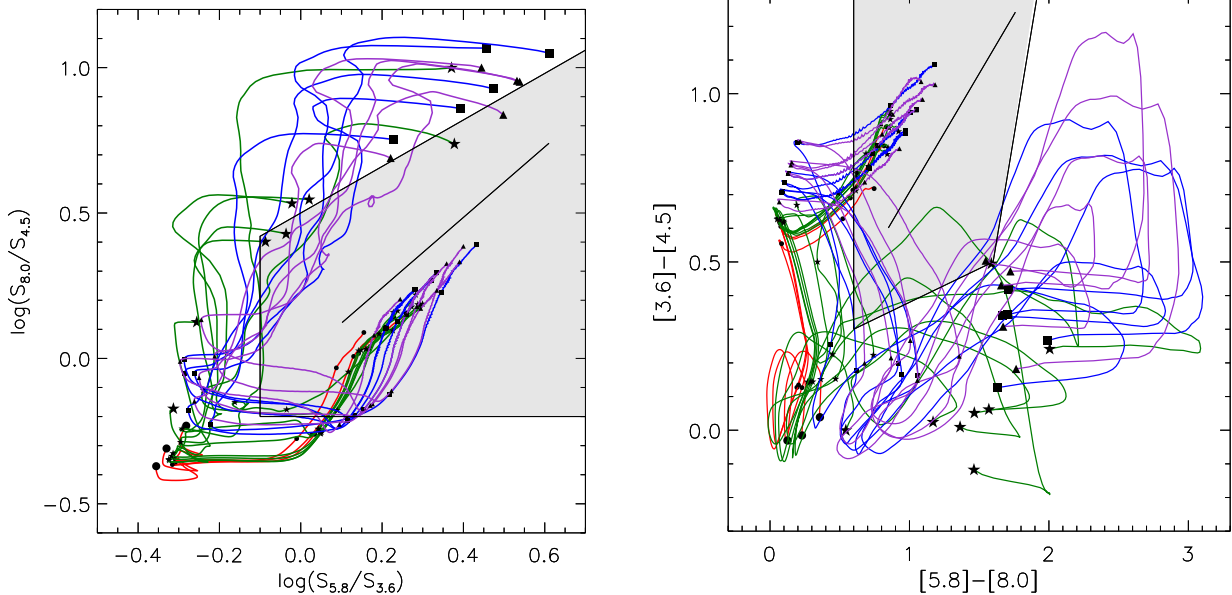


FIG. 4.— Tracks in color-space of the *purely star-forming* SEDs of ULIRGS (purple, triangles), LIRGS (blue, squares), spirals and starbursts (green, stars), and elliptical galaxies (red, circles), from redshifts of $z = 0$ (large symbols) to $z = 4$. Small symbols mark redshift intervals of 1. The power-law locus with $\alpha = -0.5$ to -3.0 is shown as a line inside the shaded AGN selection regions. The star-forming SEDs enter the AGN selection regions at both low and high redshift.

of lower luminosity ones. By $z = 1$, the typical *Spitzer* 24 μm survey sensitivity limit reaches only to the bottom of the LIRG range, so the Lacy AGN color wedge is more susceptible to contamination than was concluded by Sajina et al. (2005).

5.3. Redshift-dependent color selection

While the star-forming templates appear to trace quite well the positions of many of the color-selected galaxies in color-color space, Figure 4 covers a wide range of redshifts ($z = 0 - 4$). To understand better the overlap between the star-forming templates and the color-selected galaxies (and PLGs), we must take the redshift information into account. We therefore break the sample down into smaller redshift bins, as shown in Figures 5 and 6. We overplot on the color-color diagrams the redshift-appropriate colors of purely star-forming galaxies. To simplify the plots, we do not plot each galaxy track separately, as was done in Figure 3, but instead draw 1σ contours around the tracks, where σ is taken to be the median IRAC measurement error of the full MIPS sample. We find that, unlike the PLGs, the majority of the color-selected AGN candidates fall within or very close to the contours for star-forming galaxies of similar redshifts. Thus, it is likely that their mid-IR SEDs are dominated by star formation. This result suggests that simple mid-IR color-color cuts cannot identify reliable AGN samples without also including redshift-based or additional SED (e.g. power-law) criteria. We discuss in Appendix B the individual redshift intervals.

The summary of our findings can be found in Table 3, where we present the overall fraction of color selected galaxies and PLGs that lie outside the 1, 2, and 3σ star-forming contours. The top half of the table gives the fractions assuming no errors on the photometric redshifts; the lower half incorporates 10% errors which for clarity are imposed on the templates rather than on the individual galaxy measurements. For the PLGs, we give

two percentages: the fraction of sources that lie outside the star-forming contours in Lacy and Stern color-space, respectively.

As is clear from Table 3, the fraction of color-selected galaxies that lie outside the star-forming contours is lower than that of the PLGs by a factor of 2-10 at all three levels of significance. For instance, while 57% - 71% of PLGs lie more than 3σ from the star-forming contours in Lacy color space, the same can be said for only 5%-10% of the color-selected galaxies. In addition, increasing the significance from 1σ to 3σ has a far greater effect on the reliability of the color-selected galaxies than on that of the PLGs, especially in Lacy color-space, indicating that the color-selected galaxies lie noticeably closer to the star-forming templates than do the PLGs, as expected. We note that this analysis depends on the templates being used, as the addition or removal of any one star-forming template will result in changes in the numerical results presented above and in the table. The overall trends discussed above, however, will remain the same.

5.4. Properties of Color-selected AGN candidates

While the majority of color-selected AGN candidates lie inside the star-forming contours (see Table 3), a number of non-power-law color-selected galaxies meet the AGN selection criteria and have colors inconsistent with those of our star-forming templates. Are these AGN, as predicted? How do their redshift distributions, X-ray detection fractions, and numbers compare to those of the PLGs? In the following discussion, we define as 'secure' color-selected galaxies (and PLGs) those AGN candidates that lie $> 1\sigma$ away from the redshift-appropriate star-forming templates.

As discussed above, and as shown in Figure 2, the redshift distributions of the color-selected sources show a strong peak at $z = 2.0$, attributed to the 7.7 μm aromatic feature, a star-formation indicator. In contrast,

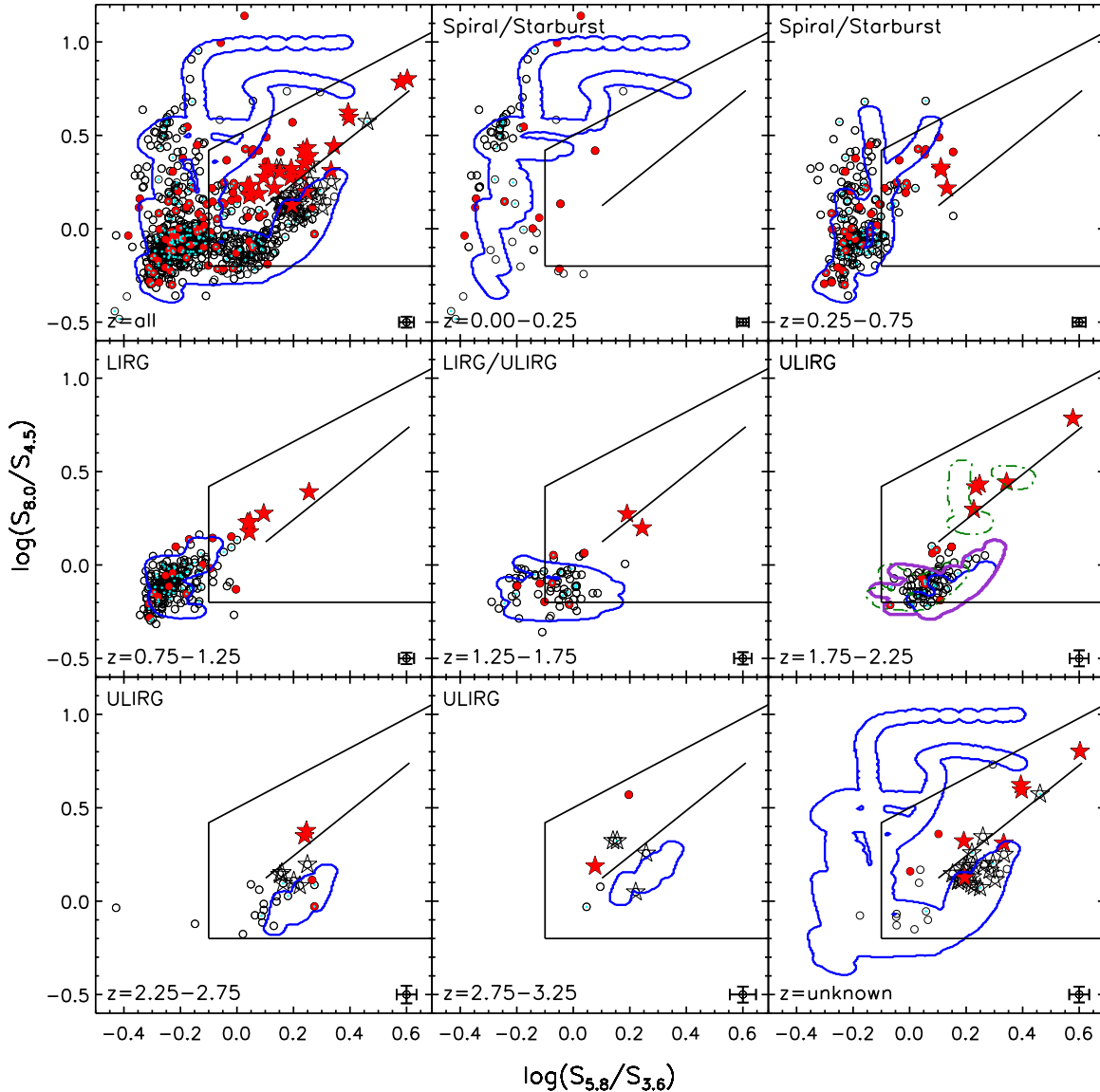


FIG. 5.— Position in Lacy et al. (2004) color-space of the MIPS-selected sample, as a function of redshift, where PLGs are shown as stars, X-ray-cataloged sources are given by filled (red) symbols, and X-ray weakly-detected sources are given as small cyan symbols. Overplotted are the redshift-appropriate contours representing the IRAC colors of purely star-forming templates, assuming no errors on the photometric redshifts. The thick (purple) contours and dot-dashed (green) contours in the $z = 1.75 - 2.25$ redshift bin represent star-forming galaxy templates for which 10% errors were incorporated into the redshift range, and AGN templates, respectively.

the PLGs have a relatively flat redshift distribution, indicating little or no contribution from aromatic features. If we do not account for errors in the photometric redshifts, the resulting sample of ‘secure’ color-selected galaxies retains the large $z = 2$ peak, suggesting a large star-formation contribution. If we incorporate 10% errors on the redshifts of the star-forming templates when selecting our secure candidates, however, the redshift distributions of the remaining color-selected galaxies become relatively flat, with mean redshifts of $z = 1.59 \pm 0.83$ and $z = 1.62 \pm 0.84$ for the Lacy and Stern-selected sources, respectively, suggesting that a significant fraction of the high-redshift star-forming contaminants have been removed. For comparison, the mean redshifts and rms ranges of the secure PLGs selected in Lacy and Stern color-space are 1.98 ± 0.87 and 2.09 ± 0.78 .

While the redshift distribution therefore suggests that many of the star-forming contaminants have been re-

jected from the secure sample, the X-ray detection fractions, shown in Table 4, suggest otherwise. At distances of 1 and 2 σ from the star-forming templates, the X-ray detection fraction of the PLGs exceeds that of the color-selected galaxies by factors of $> 2 - 3$. This factor, however, should be taken with reservations; X-ray sources are far more likely to have spectroscopic redshift estimates, and are therefore far more likely to be included in our secure sample, which requires redshift information. While this has a minimal effect on the color-selected galaxies, for which the redshift completeness is high, it has a large effect on the PLGs, boosting their probable X-ray detection fraction.

A better comparison is therefore with the IR-normal galaxy population, 11% of which are detected in the X-ray. The X-ray detection fractions of the secure color-selected AGN candidates (14-29%), exceed this value, but only by a factor of $\sim 1 - 3$. In comparison, the

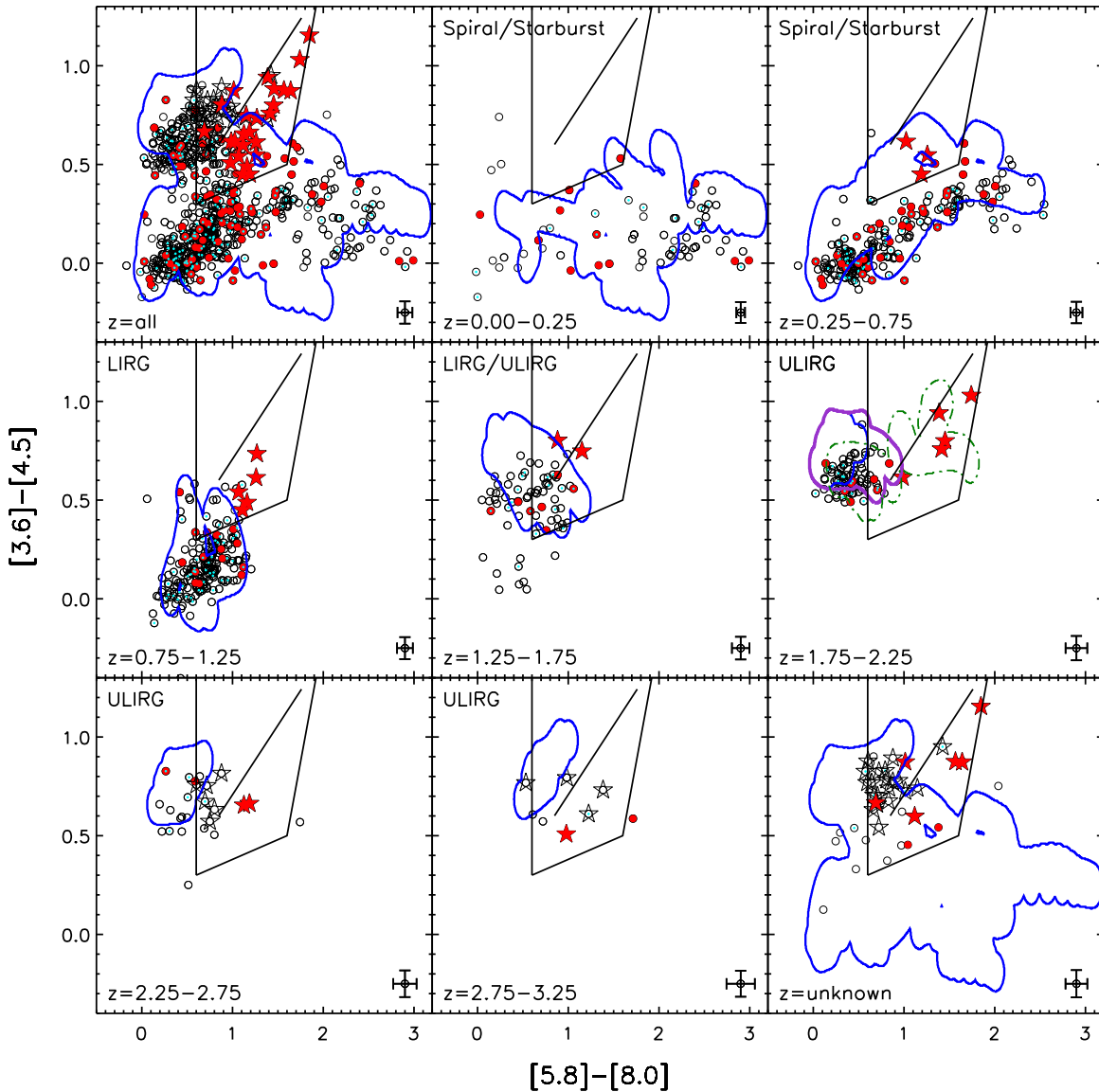


FIG. 6.— Position in Stern et al. (2005) color-space of the MIPS-selected sample, as a function of redshift. Symbols and contours are as described in Figure 5.

full sample of PLGs has an X-ray detection fraction of 45%, which exceeds that of the IR-normal galaxies by a factor of 4. Only at the highest significance, 3σ from the star-forming contours, does the X-ray detection fraction of the secure color-selected galaxies approach that of the full PLG sample.

This significant offset in X-ray detection fraction could be due either to a difference in intrinsic luminosity or to lingering contamination of the color-selected sample by star-forming galaxies. While the average X-ray luminosity of the secure PLGs, $\log L_x(\text{ergs s}^{-1}) = 44.1$, exceeds that of the secure Lacy and Stern-selected sources detected in the X-ray, $\log L_x(\text{ergs s}^{-1}) = 43.8$ and 43.9 , respectively, the offset is relatively small, suggesting that the large discrepancy in the X-ray detection fractions is not driven primarily by a systematic offset in X-ray luminosity of the relevant AGN. Instead, it likely arises from the inclusion of star-forming galaxies, even in the 1σ 'secure' color-selected population, suggesting that a larger cut in σ (e.g. 3σ) is required to define a reasonably secure

sample.

Also shown in Table 4 are the total number of X-ray selected galaxies in both the secure color-selected and PLG samples. After applying completeness corrections for the fraction of Lacy, Stern, and PLG X-ray sources that have redshifts and that can therefore be included in the secure sample (94%, 83%, and 76%, respectively), the number of secure X-ray selected PLGs exceeds that of the secure X-ray-detected color-selected galaxies, regardless of whether we define the secure sample as those sources that lie 1, 2, or 3σ from the star-forming contours. This indicates that *the PLG selection criterion identifies the overwhelming majority of secure AGN candidates in IRAC color-space.*

5.5. Flux dependency of color selection

While the Lacy and Stern AGN selection criteria were defined using relatively shallow surveys, these selection techniques are now being applied to samples with a range of flux densities (e.g. Cardamone et al. 2008). How does

the limiting flux affect the completeness and reliability of AGN color selection? Are the problems discussed above present in shallow as well as deep surveys?

There are several reasons why we might expect to see a shift in reliability with flux. First, the AGN fraction of MIPS sources depends quite strongly on the $24\ \mu\text{m}$ flux density (e.g. Treister et al. 2006, Brand et al. 2006). For instance, while only $\sim 4\%$ of MIPS sources at our flux limit of $80\ \mu\text{Jy}$ are expected to be AGN (Treister et al. 2006), the fraction at $5\ \text{mJy}$ is more than an order of magnitude greater ($\sim 45\%$). Therefore, MIPS-selected shallow surveys should contain fewer star-forming galaxies, although those that remain are likely to be LIRGs/ULIRGs that enter the AGN selection region in greater numbers than spirals and starbursts (see Figure 4).

Second, many of the ‘problem’ sources that lie inside the AGN color selection region but that also fall inside the star-forming contours have moderately high-redshifts ($z > 1.25$), and are therefore likely to drop out of shallow surveys. While shallow samples may therefore contain high-luminosity ULIRGS, the exclusion of lower-luminosity high-redshift galaxies reduces the risk of contamination. Other flux cuts, such as the R magnitude < 21.5 requirement of Stern et al. (2005), also prevent contamination at high- z , as normal galaxies at this magnitude are detected only to $z \sim 0.6$.

To investigate the effect of intermediate flux density cuts on the AGN color selection, we show in Table 5 the fraction of ‘secure’ color-selected and PLGs (those that lie outside the 1σ star-forming contours) as a function of flux density. If we do not incorporate errors in the photometric redshifts into our definition of the secure sources, we find that the fraction of secure sources is relatively constant at $\sim 50\%$ regardless of flux density. If we allow errors on the photometric redshifts when constructing our ‘secure’ sample, the reliability of Lacy-selected sources at $f \geq 80\ \mu\text{Jy}$ drops to 29% , and that of Stern-selected sources drops to 21% . At $f \geq 500\ \mu\text{Jy}$, the fraction of secure sources amongst both samples rises, but only to 50% . Regardless of our assumptions, therefore, the fraction of potential contaminants is still high ($\sim 50\%$), even at the highest fluxes probed by our survey. Because of the pencil-beam nature of the CDF-S survey, 95% of the sources in our sample have $f_{24\ \mu\text{m}} \leq 600\ \mu\text{Jy}$, so our ability to comment on brighter samples is limited.

It is also worth noting that the brightest MIPS sources tend to lie above the power-law locus in Lacy color-space and to the right of the power-law locus in Stern space, regions where we expect minimal contamination from star-forming galaxies. Not surprisingly, these sources are also almost always detected in the X-ray, suggesting that these regions of IRAC color-space are the most secure.

5.6. Comparison with previous work

In a study of 77 AGN candidates selected from the *Spitzer* First-Look (Lacy et al. 2005) and SWIRE surveys (Lonsdale et al. 2003) via the Lacy et al. (2004) criteria, Lacy et al. (2007) found that 33% are unobscured type 1 quasars, 44% are type 2 AGN, and 14% are dust-reddened type 1 quasars. Only 9% have star-forming or LINER spectra. Is this relatively low contamination by star-forming galaxies consistent with our findings?

There are three main factors that lead to the high reli-

bility of the Lacy et al. (2007) sample. First, the sample members are very bright, with a typical $24\ \mu\text{m}$ flux density of $5\ \text{mJy}$. As discussed above, Treister et al. (2006) predict that 45% of sources at this flux density should be AGN, regardless of their MIR SEDs, compared to only 4% of sources at our flux limit of $80\ \mu\text{Jy}$. Indeed, of the brightest 50 sources in the XFLS (whose median $24\ \mu\text{m}$ flux density is $9.4\ \text{mJy}$), 58% are optically classified as AGN (Lacy et al. 2007). Thus, the sample from which these color-selected AGN was drawn contains far fewer star-forming galaxies than the deeper GOODS sample.

Second, while the sources in the Lacy et al. (2007) sample have redshifts ranging from $z = 0.053$ to 4.27 , the median redshift of the sample is low: $z = 0.6$. Only 5 color-selected sources have redshifts in excess of $z = 1.75$, the redshift above which nearly all sources in our sample (AGN or star-forming) meet the Lacy et al. criteria. We would therefore expect little or no contamination by *high-redshift* star-forming galaxies, the predominant source of contamination in our faint sample.

The third and most important reason for the high reliability of this sample, however, is the high PLG fraction of the Lacy-selected AGN candidates. Of the 77 sources in the Lacy et al. (2007) sample, 59 are PLGs as defined in §2. The 18 sources that are excluded by the PLG criteria include the only two starburst galaxies detected in this subsample, one starburst/LINER, an unclassified high-redshift galaxy with narrow UV emission lines, two composite galaxies, 8 Type 2 AGN (the identification of 4 of which were based on a BPT analysis), 3 reddened Type 1 AGN, and 1 Type 1 AGN. If we relax the probability constraint of the PLG criterion to $P\chi > 0.01$, as was done in Alonso-Herrero et al. (2006), we recover 69 of the 77 Lacy et al. (2007) sources selected for optical follow-up. Excluded are the two starburst galaxies, one high- z unidentified galaxy, three Type 2 AGN, one reddened Type 1 AGN, and 1 Type 1 AGN whose slope of $\alpha = -0.41$ falls just short of our cut of $\alpha \leq -0.5$. The high reliability of this luminous color-selected sample is therefore consistent with our findings in §6 that while non-PLG color-selected AGN are subject to contamination by star-forming galaxies, sources selected via a power-law criterion are reliable.

6. IRAC POWER-LAW SELECTION

Thus far, we have focused primarily on the reliability of the AGN color selection criteria of Lacy et al. (2004) and Stern et al. (2005). In doing so, we have separated out the subset of sources that meet the power-law criteria of Alonso-Herrero et al. (2006) and Donley et al. (2007). Here, we discuss the PLG selection itself, in particular the consequences of various choices of limiting power-law slope, α .

Our default cut of $\alpha < -0.5$ was chosen to match the spectral indices of typical AGN (e.g. Alonso-Herrero et al. 2006, Donley et al. 2007). In the optical, AGN have spectral slopes of $\alpha = 0.5$ to -2 (SDSS, Ivezić et al. 2002), with a mean value of $\alpha \sim -1$ (Neugebauer et al. 1979, Elvis et al. 1994). In the IRAC bands, broad-line AGN exhibit similar slopes, with a mean value of $\alpha = -1.07 \pm 0.53$ (Stern et al. 2005).

In Figures 7 and 8, we plot PLGs selected via cuts in α ranging from $+0.5$ to -1.5 . At high redshift ($z \sim 1.5 - 2$) the IRAC bands trace the blue side of the stellar bump.

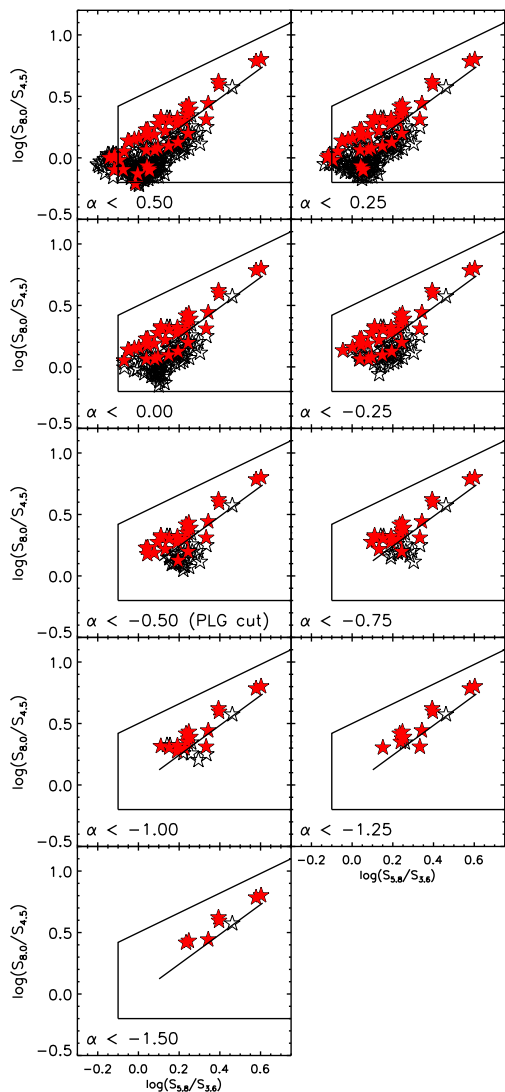


FIG. 7.— Position in Lacy et al. (2004) color space of PLGs as a function of the power-law slope cut, α . X-ray-detected sources are shown as filled (red) symbols.

It is therefore not surprising that at the bluest slopes ($\alpha = +0.5$), the PLG sample is dominated by the population of high redshift X-ray-non-detected star-forming galaxies discussed above. As the required slope reddens towards our cut of $\alpha < -0.5$, the high-redshift star-forming galaxies gradually drop out of the sample, and the X-ray detection fractions rise from 21% at $\alpha = +0.5$ to 30%, 45%, 67%, 88%, and 80% at $\alpha = 0.0, -0.5, -1.0, -1.5$, and -2.0 . While choosing a redder cut in α therefore increases the apparent reliability of the PLG selection, it also decreases the number of galaxies selected, and may exclude interesting heavily obscured, X-ray-non-detected AGN like those seen in the CDF-N (e.g. Donley et al. 2007).

The X-ray-non-detected PLGs in the current sample tend to be the faintest sources both in the IRAC bands and at $24 \mu\text{m}$, where their mean flux density, $146 \mu\text{Jy}$, is over a factor of 2 lower than that of the X-ray-detected sample, $334 \mu\text{Jy}$. The low X-ray detection fraction of these faint sources may therefore be due simply to their systematically lower fluxes. At $z > 2.6 - 2.9$, however, the star-forming ULIRG templates have IRAC SEDs that

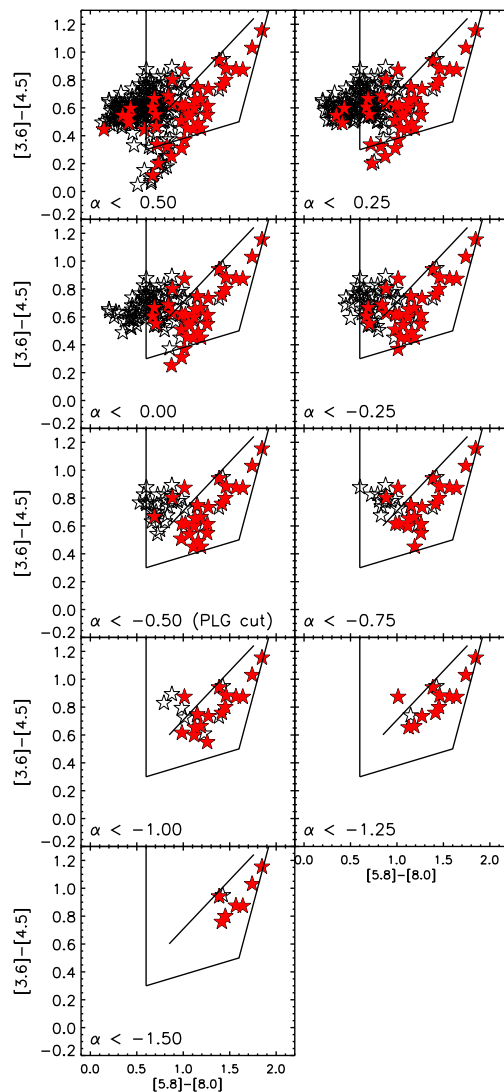


FIG. 8.— Position in Stern et al. (2004) color space of PLGs as a function of the power-law slope cut, α . X-ray-detected sources are shown as filled (red) symbols.

meet the PLG criteria, although dropping the power-law slope criterion to $\alpha \leq -1.0$ and $\alpha \leq -1.5$ raises this redshift range to $z > 2.74 - 3.92$ (depending on the template) and to $z > 3.4 - 4.2$, respectively (with the IRAS 22491-1808 template never reaching an α of -1.5). It is therefore possible that the X-ray non-detected PLGs (which tend not to have redshift estimates, to be faint, and to lie at relatively high α) are high-redshift star-forming galaxies. To test this hypothesis, we plot in Figure 9 the ratio of the MIPS $24 \mu\text{m}$ flux density to that of the $3.6 \mu\text{m}$ IRAC band. At the redshifts of interest ($z > 2.6$), this flux ratio allows a direct comparison of the hot dust emission at $5-7 \mu\text{m}$ to the stellar emission at $\sim 1 \mu\text{m}$. Overplotted on the colors of our MIPS-selected sample are the redshifted colors of the AGN templates of Polletta et al. (2007, see Table 1) and the purely star-forming LIRG and ULIRG templates of Rieke et al. (2008). The mean colors of PLGs without redshift estimates are given by large symbols placed at $z = 2.6$, the redshift above which contamination by star-forming galaxies is possible. The circle, square, and triangle represent all PLGs without redshifts, those that are detected in the X-ray, and those

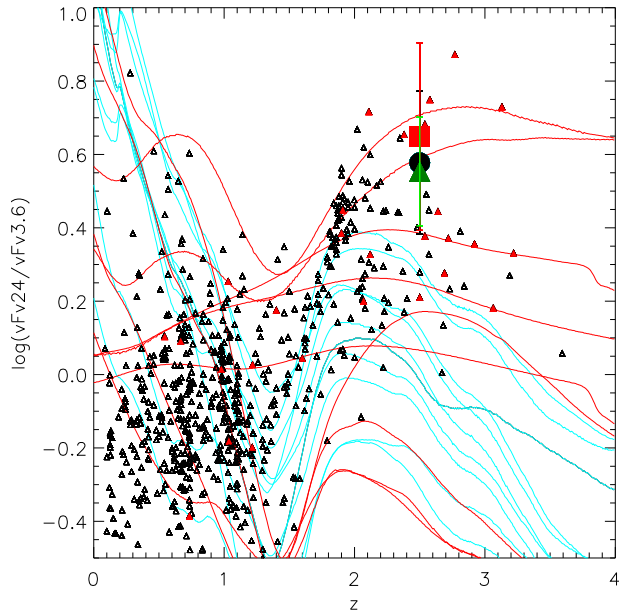


FIG. 9.— Observed $24\ \mu\text{m}$ to $3.6\ \mu\text{m}$ color as a function of redshift. The tracks represent the AGN templates of Polletta et al. (2007, red) (see Table A1), and the purely star-forming LIRG and ULIRG templates of Rieke et al. (2008, cyan). Triangles represent all sources in our sample with redshift estimates, and filled (red) triangles indicate a PLG source. The mean colors of PLGs without redshift estimates are given by a large circle (all PLGs), a large square (X-ray-detected PLGs), and a large triangle (X-ray-non-detected PLGs). We arbitrarily placed these mean colors at a redshift of $z = 2.6$, above which contamination of the PLG sample by star-forming galaxies is possible. The colors of these sources, however, are consistent with AGN, not star-forming galaxies.

that are not, respectively.

As can be seen in Figure 9, the X-ray-detected and X-ray-non-detected PLGs lacking redshifts have consistent $24\ \mu\text{m}$ to $3.6\ \mu\text{m}$ colors, suggesting that there is no significant difference between these two sub-samples. In addition, while the colors of these sources are consistent with those of AGN, they lie well above those of star-forming galaxies, not only at high redshift, but at all redshifts greater than $z \sim 0.6$. In other words, the PLGs that are undetected in the X-ray and that lack redshifts (preventing us from testing their reliability as in §5.3) appear to have more hot dust emission than can be explained by purely star-forming templates, especially at high- z where star-forming contamination of the PLG sample is most likely. This result suggests that these sources are more likely to be AGN than star-forming galaxies. Other lines of evidence, e.g. variability (Klesman & Sarajedini 2007), and X-ray properties (Steffen et al. 2007), tend to support this conclusion. In addition, we note from Figure 9 that a number of the other galaxies at $z \sim 2$ have colors slightly redder than those predicted by star-forming galaxies at this redshift. This behavior may be due to a minor issue with the templates, a small AGN contribution to the MIR flux density, or to reddening that exceeds that seen in our local LIRG/ULIRG templates.

Finally, the segregation of the X-ray-detected and X-ray-non-detected sources about the power-law locus, seen in Figures 7 and 8, warrants discussion, as this was not seen in the CDF-N (Donley et al. 2007). This behavior appears to be due largely to the different selection methods and limiting fluxes of the two samples. While the CDF-N PLG sample was selected on the basis of

IRAC fluxes, the current sample was selected from a flux-limited MIPS sample with far deeper IRAC data. If we require the CDF-S sample to meet the IRAC detection limits of the CDF-N study, the PLG sample size decreases by a factor of 2 and the X-ray detection fraction rises to 78%. The segregation in the PLG sample is also greatly reduced, due largely to the loss of many of the X-ray-non-detected sources. This high X-ray detection fraction of 78%, however, is surprising as it is significantly higher than the 55% found for the CDF-N PLG sample. To test whether this change is a result of the much improved IRAC data, we recalculated the spectral properties of the galaxies in the CDF-N using the most current IRAC data, which now includes the super-deep GOODS-N coverage not previously available. Drawing PLGs from the same initial sample used in Donley et al. (2007), we find an updated X-ray detection fraction of 57%, a value nearly identical to that found previously. For consistency with the current sample, we further restricted the PLG sample to those sources detected in the super-deep GOODS field, where the X-ray exposure is generally higher. Doing so raises the X-ray detection fraction to 65%. The remaining offset in the X-ray detection fractions of the IRAC flux-limited PLGs in the GOODS-N and GOODS-S fields, 13%, therefore appears to be due primarily to cosmic variance and small number statistics.

7. IR-EXCESS SELECTION

Both high-redshift star-forming galaxies and AGN can exhibit extremely red infrared to optical colors when heavily dust-obscured (e.g. Dey et al. 2008). While the relative fractions of AGN and star-forming galaxies among IR-excess samples is still a matter of debate, the fraction of dust-obscured galaxies (DOGs) with AGN-like power-law SEDs has been shown to decrease with decreasing flux from $\sim 70\%$ at $f = 1\ \text{mJy}$ to $\sim 20 - 25\%$ at $f \leq 300\ \mu\text{Jy}$ (Dey et al. 2008). We might therefore expect a relatively small AGN fraction amongst the faint IR-excess sources in the GOODS fields, whose mean $24\ \mu\text{m}$ flux is $215\ \mu\text{Jy}$. Fiore et al. (2008), however, estimate that 80% of their red, IR-excess galaxies are heavily obscured, Compton-thick AGN. Here, we probe the nature of the IR-excess sources and examine the overlap between the IR-excess galaxies and the X-ray, color-selected, and power-law samples discussed above.

The positions of the IR-excess galaxies in Lacy and Stern IRAC color-space are shown in Figure 10, and their overlap with the X-ray, PLG, and color-selected samples is given in Table 2. Of the 101 IR-excess sources, 24 (24%) are PLGs and all but 7 meet either the Lacy, Stern, or power-law criteria. At least 1/4 of the IR-excess galaxies therefore show evidence for AGN-heated dust (with the fraction rising to 100% for the luminous AGN selected via the Polletta et al. (2008) criteria, as expected). Not all PLGs, however, have IR-excess colors. Of the 55 PLGs, only 44% meet one or more of the IR-excess criteria. The same can be said for 33% of the IRAC color-selected galaxies, but for only 2% of the IR-normal galaxies.

Of the IR-excess sources, only 15% have cataloged X-ray counterparts, with the fraction rising to 45% when weak ($\geq 2\sigma$) X-ray detections are considered (see Table 2). Of the X-ray-cataloged sources, 47% are PLGs, 47%

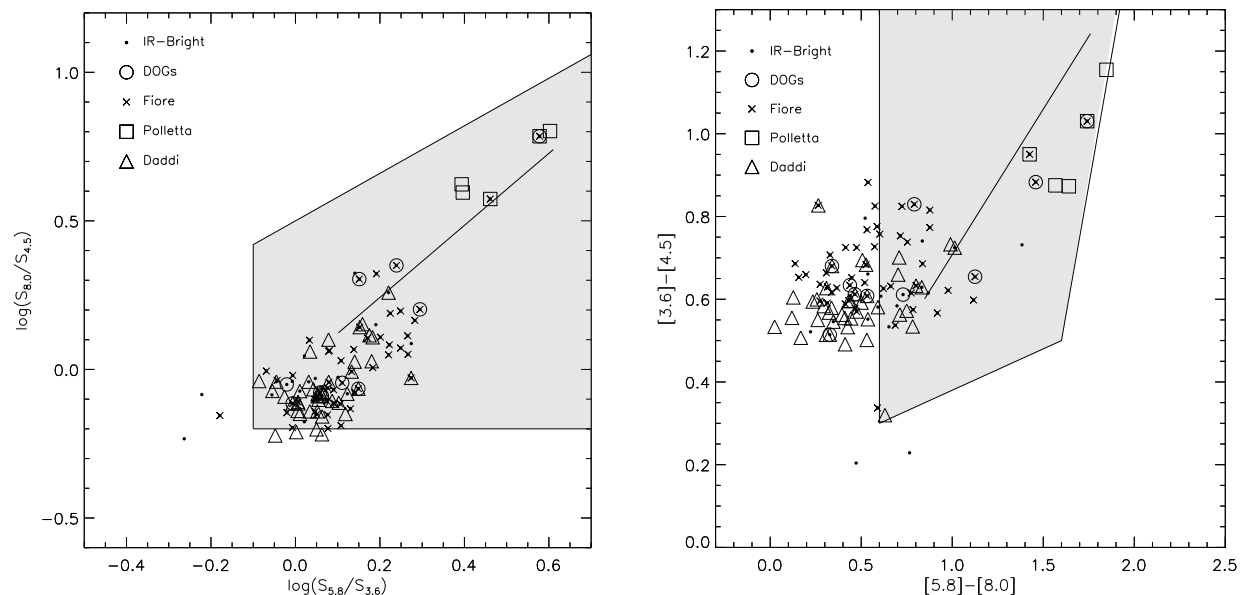


FIG. 10.— Position in Lacy et al. (left) and Stern et al. (right) color-space of the IR-excess sources.

are color-selected galaxies, and 1 (6%) is IR-normal. The statistics are quite different for those sources with no cataloged X-ray emission, where the power-law fraction drops to 19% and the color-selected fraction rises to 73%.

While a strong argument can be made for the AGN nature of the 32 IR-excess sources with cataloged X-ray counterparts and/or PLG SEDs, what can be said about the remaining IR-excess sources? As discussed in §3, the concentration of the redshifts of these sources about $z = 2$ may be due to the passage of the $7.7 \mu\text{m}$ aromatic feature through the $24 \mu\text{m}$ band, suggesting a significant contribution from star-formation. In addition, the vast majority of color-selected sources at $z = 2$ (of which these are a subset) have IRAC colors consistent with those of star-forming galaxies or low-luminosity AGN whose IRAC SEDs are dominated by the host galaxy. In combination with the lack of significant X-ray emission, these facts suggest that the remaining 68% of the IR-excess sample could be either star-forming galaxies, or extremely obscured AGN. To distinguish between these two possibilities, we consider in more detail the sources selected via the Daddi et al. and Fiore et al. criteria.

7.1. Daddi et al. (2007) Compton-thick AGN candidates

Of the 88 IR-excess AGN candidates selected in the ISAAC region of GOODS-S by Daddi et al. (2007a), the list of which was kindly provided by D. Alexander (private communication, 2008), 42 fall in our MIPS-selected sample. Twenty-three of the remaining 46 galaxies have MIPS fluxes that fall below our cut of $f_{24 \mu\text{m}} \geq 80 \mu\text{Jy}$, and 6 galaxies lack MIPS and/or IRAC counterparts in our catalogs, indicating that they too are faint. Seven galaxies were excluded because of observable blending in the MIPS or IRAC bands, and an additional 10 were removed from our sample because of multiple optical counterparts.

The positions of the Daddi et al. sources in IRAC color-space are shown in Figure 10. Thirty-eight of the

42 Daddi et al. sources in our sample meet the Lacy et al. IRAC color-selection criteria. Only 10 meet the Stern et al. AGN selection criterion, and only 5 are PLGs (4 of which have relatively shallow slopes of only $\alpha \sim -0.6$). In addition, only 15 (36%) meet any of the other IR-excess criteria. This is not surprising, as the MIR emission from the Daddi et al. IR-excess sources exceeds that of a typical star-forming galaxy by a factor of only $\gtrsim 3$ (Daddi et al. 2007b). Of the 42 IR-excess galaxies, 18 have IRAC colors that lie $> 1\sigma$ from the redshift-appropriate star-forming contours in either Lacy or Stern color-space. Only 3 and 1, however, have colors that lie outside the 2σ and 3σ contours, respectively. As discussed above, however, this indicates only that any AGN activity can not be identified on the basis of the MIR IRAC colors alone.

To determine the nature of the Daddi et al. (2007) sources in our sample, we therefore turn to the X-ray data. While none of the IR-excess galaxies are individually detected in the hard X-ray band (by definition), 3 have soft X-ray detections and 13 have faint ($> 2\sigma$) X-ray counterparts. Twenty remain X-ray-undetected, and 6 sources have a nearby X-ray counterpart that prevents an accurate test for low- σ X-ray flux. Using the procedure outlined in Steffen et al. (2007), with the only change being our slightly different choice of source aperture radius, $2''$, we coadded the three sources detected in the soft band, whose soft-band luminosities of $L_x > 10^{42} \text{ ergs s}^{-1}$ indicate that they are AGN. We verify that our stacking method reproduces the results of Daddi et al. (2007b) for the same sample of 59 IR-excess galaxies used in that work. While the coaddition of the 3 soft X-ray detected sources did not lead to a hard band detection, we place a 3σ limit on the hard-band flux that constrains their column density to $N_H \lesssim 2 \times 10^{22} \text{ cm}^{-2}$, assuming an intrinsic photon index of $\Gamma = 1.8$.

A coaddition of the 13 weakly-detected sources leads to a 3.3σ hard-band detection, a 9.7σ soft-band detection, a hardness ratio of $HR = -0.31$, and a photon index of $\Gamma = 1.4$. If we assume that these sources are

AGN at their mean redshift of $z = 1.81$, the hard to soft flux ratio corresponds to an obscured column density of $N_{\text{H}} = 3.6 \times 10^{22} \text{ cm}^{-2}$. At this modest obscured yet Compton-thin column density, the observed soft band flux is only attenuated by a factor of 2, implying that the sources must have relatively low luminosities. Indeed, the rest-frame 2-10 keV absorption-corrected luminosity derived from the observed soft-band flux is only $L_{\text{x}} = 1.6 \times 10^{42} \text{ ergs s}^{-1}$.

However, Daddi et al. (2007b) argue that the coadded soft X-ray flux of their full IR-excess sample can be attributed to star-formation. When they subtract this component from the detected fluxes, the hardness of the remaining X-ray emission implies a significantly larger (e.g. Compton-thick) column density as well as a larger absorption-corrected luminosity.

To test the origin of the X-ray emission, we plot in Figure 11 the 2-10 keV luminosity and $25 \mu\text{m}$ power (νL_{ν}) of a sample of starburst and AGN-dominated galaxies and ULIRGs drawn from Franceschini et al. (2003), Ranalli et al. (2003), and Persic et al. (2004). The $25 \mu\text{m}$ luminosities were extracted from the IRAS Revised Bright Galaxy Sample (RBGS, Sanders et al. 2003) when available, and from ISO (Klaas et al. 2001) or the IRAS Faint Source Catalog otherwise. As both the hard X-ray and MIR flux densities of star-forming galaxies trace the current star-formation rate (e.g. Ranalli et al. 2003, Franceschini et al. 2003), these two luminosities are well correlated for starbursts and starburst-dominated ULIRGs (though there is a hint of a turnover to lower X-ray luminosities amongst the ULIRG sample). AGN, however, show an increased X-ray output for their observed $25 \mu\text{m}$ flux density.

To compare the Daddi et al. sample to these local starburst and ULIRG samples, we convert the observed soft-band (rest frame $\sim 1.5\text{--}6 \text{ keV}$) luminosity to a rest-frame 2-10 keV luminosity, and the observed $70 \mu\text{m}$ (rest-frame $\sim 23 \mu\text{m}$) flux density given by Daddi et al. (2007b) to a rest-frame $25 \mu\text{m}$ power. The mean luminosities of the full Daddi et al. (2007b) IR-normal and IR-excess samples fall on the best-fit correlation for star-forming galaxies, confirming that their observed soft X-ray flux can be attributed to star-formation. The X-ray luminosity of the X-ray weakly-detected IR-excess galaxies in our MIPS sample, however, is somewhat higher than predicted. The AGN origin of the soft X-ray emission is supported by the 2-10 keV luminosity implied by the soft X-ray flux, $L_{\text{x}} = 1.6 \times 10^{42} \text{ ergs s}^{-1}$. If the soft X-ray flux has a significant contribution from the AGN, then it cannot all be subtracted from the AGN spectrum, resulting in column densities lower than estimated by Daddi et al. (2007b).

However, the indicated AGN contribution is modest, and is based on an average. Therefore, it is likely that there will be a significant range of star-formation-corrected absorbing columns, including some that are Compton thick. Indeed, Alexander et al. (2008) show that a sample of 6 spectroscopically-confirmed Compton-thick AGN would be selected via the Daddi et al. (2007) method, although 4 of the 6 have infrared excesses of a factor of > 100 , and thus represent the most extreme IR-excess sources.

A coaddition of the 20 X-ray non-detected Daddi et al. sources in our sample leads only to a marginal 2.0σ

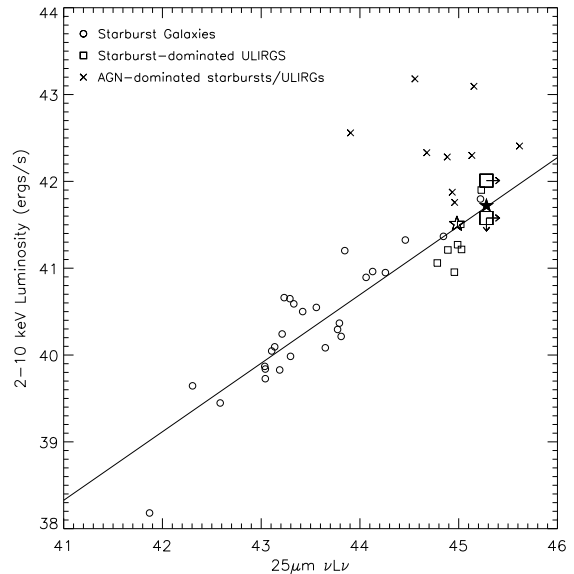


FIG. 11.— Rest-frame 2-10 keV luminosity vs. rest-frame $25 \mu\text{m}$ power. The small symbols represent the starburst and ULIRG samples of Franceschini et al. (2003), Ranalli et al. (2003), and Persic et al. (2004), where starburst dominated sources are given as squares and circles, and AGN-dominated sources are given by crosses. The solid line gives the best-fit linear relationship between the X-ray and $25 \mu\text{m}$ luminosities of the star-formation-dominated sources. The large filled and open stars represent the full IR-excess and IR-normal samples from Daddi et al. (2007b), respectively, and the large squares represent the X-ray weakly- and non-detected members of the Daddi et al. sources in our sample. Because these sources comprise the brighter subset of the full Daddi et al. sample, we treat the full $25 \mu\text{m}$ flux density (derived from the coadded $70 \mu\text{m}$ flux density given by Daddi et al. (2007b)) as a lower-limit.

detection in the full band ($0.5\text{--}8 \text{ keV}$), and 1.8σ and 1.0σ detections in the hard and soft bands, respectively. A 3σ limit on the soft flux gives a 2-10 keV luminosity of $L_{\text{x}} \leq 3.8 \times 10^{41} \text{ ergs s}^{-1}$, fully consistent with a star-forming origin (see Figure 11). (The 2-10 keV luminosity derived from the marginal full-band detection is even lower: $L_{\text{x}} \leq 2.2 \times 10^{41} \text{ ergs s}^{-1}$). The near-detection in the hard-band, however, suggests that these sources may have relatively hard X-ray spectra. By coadding the weakly and non-detected sources, the photon index drops to $\Gamma = 1.04^{+0.16}_{-0.14}$, from a value of $\Gamma = 1.39^{+0.21}_{-0.17}$ measured for the weakly-detected sources. There is therefore marginal (1σ) evidence that the X-ray non-detected sources have spectra harder than those of their weakly-detected counterparts. Does this hard spectrum confirm that these sources are AGN, or might there be another explanation?

7.1.1. A Star-formation Origin?

While it is well-known that heavily obscured AGN exhibit hard X-ray spectra, star-forming galaxies can also produce such spectra. As discussed in Persic & Rephaeli (2002) and Persic et al. (2004), the hard ($> 2\text{--}10 \text{ keV}$) X-ray emission of star-forming galaxies is dominated by low and high-mass X-ray binaries (LMXBs, HMXBs), with the HMXB fraction increasing from $\sim 20\%$ at starburst luminosities to $\sim 100\%$ at ULIRG luminosities. As shown by White, Swank, & Holt (1983), HMXBs have X-ray spectra with $\Gamma = 1.2 \pm 0.2$, a cutoff energy of 20 keV , and an e -folding energy of $\sim 12 \text{ keV}$ (see e.g. Persic & Rephaeli 2002). At $z = 2$, the $0.5\text{--}2 \text{ keV}$ and $2\text{--}8 \text{ keV}$

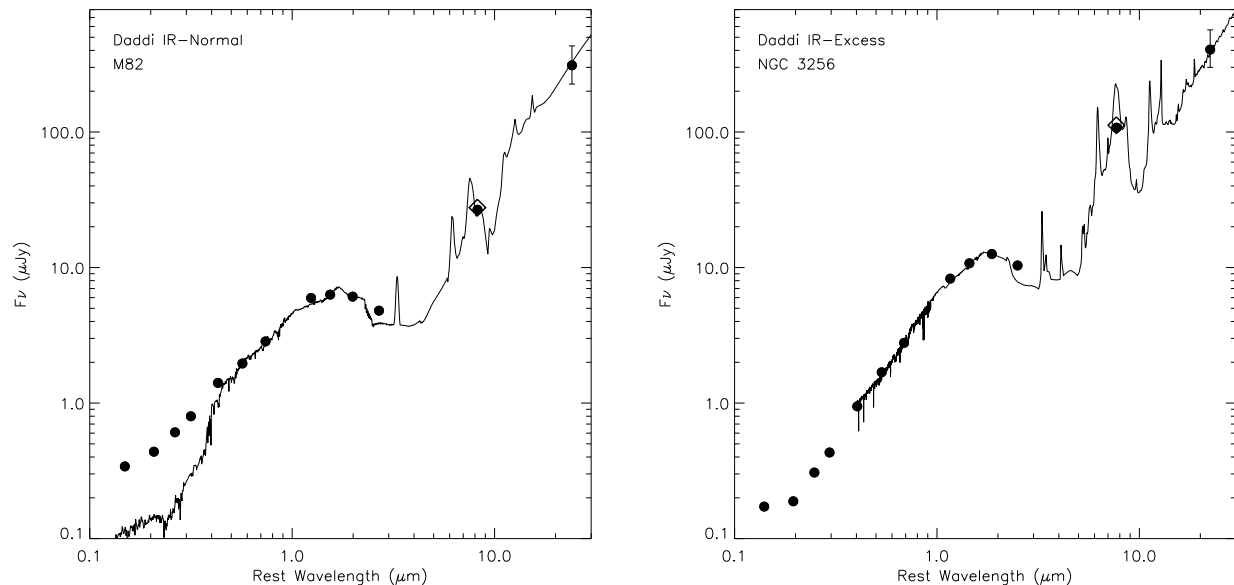


FIG. 12.— Median SEDs of the full Daddi et al. (2007a,b) IR-normal and IR-excess GOODS-S samples, as given in Figure 4 of Daddi et al. (2007b). Overplotted are the *purely star-forming* SEDs of the starburst galaxy M82 (left) and LIRG NGC 3256 (right) (The Rieke et al. (2008) templates only extend down to $\sim 0.4 \mu\text{m}$). We have applied an additional reddening of $A_V = 0.8$ to the NGC 3256 template. The open diamonds represents the flux that would be measured in the MIPS $24 \mu\text{m}$ band when the bandpass is convolved with the SED. The optical-MIR SEDs of both the IR-normal and IR-excess sources are well-fit by star-forming SEDs.

X-ray bands sample the rest-frame 1.5-6 keV and 6-24 keV X-ray bands, and therefore should be minimally affected by the power-law cutoff. A luminous star-forming galaxy undergoing an isolated burst of star-formation is therefore expected to display a hard X-ray spectrum of $\Gamma = 1.0 - 1.4$ over the energies observed in our sample. X-ray binary emission has been proposed as an explanation for the hard ($\Gamma \sim 1.0$) spectrum of Arp 220 (Iwasawa et al. 2001), the spectra of the apparently starburst-dominated ULIRGS of Ptak et al. (2003) and Teng et al. (2004), whose photon indices tend to lie at $\Gamma = 1.0 - 1.5$, and the starburst-dominated ULIRGS of Franceschini et al. (2003).

While the hard X-ray properties of the IR-excess sources do not therefore require an AGN origin, can the same be said of their MIR properties? To test the nature of these sources, we first plot in Figure 12 the median SEDs of the full GOODS-S IR-normal and IR-excess samples, as given in Figure 4 of Daddi et al. (2007b). Although these high-redshift sources appear to be highly luminous (see Figure 11), there are indications that local templates for lower-luminosity galaxies are appropriate for them, at least in the optical-MIR (Rigby et al. 2008). It is therefore not surprising that the optical-MIR SED of the IR-normal galaxies is well-fit by the M82 SB template of Polletta et al. (2007). (The discrepancy between the observed SED and template at shorter wavelengths is likely due to a difference in the reddening and/or age of the stellar population.) The IR-excess SED is also very well fit by the *purely star-forming* template of the LIRG NGC 3256 (Rieke et al. 2008), to which we have applied an additional reddening of $A_V \sim 0.8$. While this does not rule out an AGN contribution to the Daddi et al. IR-excess sample, it does indicate that an AGN need not be present to produce the observed SEDs of the IR-excess sources, and that their IR-excesses may simply be due to strong aromatic emission associated with their systematically higher IR luminosities, as suggested by Daddi et

al. (2007a).

If these IR-excess sources are dominated by star-formation, then it appears either that their IR SFRs have been overestimated or that their UV-derived SFRs have been underestimated. The former scenario could be partially attributed to the larger than unity slope between $24 \mu\text{m}$ luminosity and $\text{Pa}\alpha$ -derived SFR (Alonso-Herrero et al. 2006, Calzetti et al. 2007), which indicates that as the SFR increases, an increasing fraction of the resulting light is emitted in the MIR. A simple proportional relationship between SFR and IR luminosity (e.g. that of Kennicutt 1998) will therefore increasingly overpredict the SFR for more luminous infrared galaxies.

An underestimate in the UV-derived star-formation rates could be due to the inherent difficulties in determining accurate UV SFRs for luminous, heavily obscured galaxies (e.g. Goldader et al. 2002, Buat et al. 2005). While UV extinction is known to correlate with luminosity (see Goldader et al. 2002; Vijh, Witt, & Gordon 2003; Buat et al. 2005), Daddi et al. (2007a) find no difference between the average derived A_{1500} values of the IR-normal and IR-excess samples, despite the systematically higher $8 \mu\text{m}$ luminosities of the IR-excess sample (see Figure 2 of Daddi et al. 2007b). Under the assumption that the radio emission arises purely from star-formation, the radio luminosities of the 16 radio-detected IR-excess galaxies similarly indicate the UV SFRs have been underestimated by a mean factor of 6.4, and a median factor of 3.5 (see Figure 12 of Daddi et al. 2007a). A stack of all IR-excess galaxies, however, leads to radio SFRs that are consistent with those derived in the UV.

7.1.2. Summary

We have divided the 42 Daddi et al. IR-excess galaxies in our MIPS-selected sample into three subsamples: those that are X-ray detected (3), those that are weakly-detected in the X-ray (13), and those that remain undetected in the X-ray down to 2σ (20). (The remaining 6

sources lie too close to an X-ray source to test for faint emission.) The 3 X-ray detected sources are AGN with $L_x > 10^{42}$ ergs s $^{-1}$, but have relatively low obscuration ($N_H \leq 2 \times 10^{22}$ cm $^{-2}$).

A coaddition of the weakly-detected sources leads to a hard ($\Gamma = 1.4$) X-ray detection. If these sources are obscured AGN, the hardness ratio implies a column density of $N_H = 3.6 \times 10^{22}$ cm $^{-2}$. A hard detection, however, could be attributed either to obscured AGN activity or to star-formation via HMXBs. Furthermore, the median SED of the full Daddi et al. (2007b) IR-excess sample is consistent with that of a local star-forming LIRG, suggesting that the MIR emission alone also cannot be used to rule out a star-forming origin. A comparison of the X-ray and MIR luminosities of these weakly-detected sources does not conclusively distinguish between a star-forming or AGN origin for the X-ray emission. There are therefore 3 possible explanations for the members of this sample of IR-excess galaxies: (1) the sources are Compton-thick AGN whose soft X-ray emission can be attributed to star-formation and whose hard X-ray emission comes from the AGN, (2) they are relatively low-luminosity, Compton-thin AGN, whose soft X-ray emission can not be entirely attributed to star-formation, or (3) they are star-forming galaxies whose soft and hard X-ray emission arise from star-formation. While the derived 2-10 keV X-ray luminosity of $\sim 10^{42}$ ergs s $^{-1}$ suggests explanation (2), it is not sufficiently high to definitively rule out the remaining scenarios. It is likely that no single possibility applies to all 13 galaxies, but that the possibilities define the range of their behavior.

The X-ray non-detected sources, when coadded alone and with the X-ray weakly-detected sample, also appear to have a relatively hard X-ray spectrum. Their X-ray luminosity, however, is significantly lower than that of the weakly-detected sources, $L_x \leq 3.8 \times 10^{41}$ ergs s $^{-1}$. If the hard spectrum arises from HMXBs, the properties of this sample would be consistent with a star-formation origin.

In summary, while we cannot rule out an obscured AGN origin for the Daddi et al. IR-excess sources in our MIPS-selected sample, their properties may also be consistent with a purely star-formation origin in the majority of cases. Further analysis, taking into account the additional 1 Ms of X-ray exposure in the CDF-S, is therefore required to establish their nature.

7.2. *Fiore et al. (2008) Compton-thick AGN candidates*

Fiore et al. (2008) select IR-excess galaxies with the following properties: $f_{24 \mu\text{m}}/f_R \geq 1000$ and $R - K > 4.5$. Using the MUSIC catalogs (see §2.3), we selected 64 sources that meet these criteria and that have 24 μm flux densities $> 80 \mu\text{Jy}$. However, 9 of these sources were removed from our MIPS sample because of visible blending in the MIPS and/or IRAC bands (see §2), which may have been responsible for their anomalously high IR to optical flux ratios (unlike Grazian et al. (2006), we do not attempt to de-blend such sources). A visual inspection of the remaining sources led to the removal of 3 additional sources with blended K-band fluxes, leaving 52 high-quality IR-excess sources.

The first Fiore criterion was designed to select obscured AGN with large X-ray to optical flux ratios (see their

Figure 2) whose column densities tend to range from $N_H = 10^{22}$ to 10^{23} cm $^{-2}$ (see Fiore et al. 2008 and references therein). The $R - K$ criterion ensures that only extremely red objects (EROs) fall in the sample. The AGN amongst ERO samples tend also to be X-ray obscured with $N_H = 10^{22} - 10^{24}$ cm $^{-2}$ (Brusa et al. 2005). Obscured AGN are therefore likely to be targeted by these criteria. However, these two selection criteria are known to identify both AGN and star-forming galaxies (e.g. Alexander et al. 2002, Doherty et al. 2005, Dey et al. 2008). We therefore examine whether these criteria are sufficiently stringent to exclude the possibility that the properties of these sources could arise from star formation.

The first of the three main arguments for the Compton-thick AGN nature of the Fiore et al. sources is the ability of the obscured AGN template of IRAS 09104+41091 (Pozzi et al. 2007) to reproduce the extreme colors of these sources, and the comparable inability of the M82 and Arp 220 star-forming templates to do the same (see their Figure 3). When fitting SEDs to the sources in their sample, Fiore et al. find that only 36% of their X-ray non-detected sources are best-fit by elliptical, spiral, M82, N6090, or Arp 220 star-forming templates. Of the sources in our MIPS-selected sample that meet the Fiore et al. criteria and have good redshift fits, we find an even lower fraction of sources best-fit by these templates: 20%. However, as shown in Figure 13, the purely star-forming IRAS 22491 template of Polletta et al. (2007) satisfies the Fiore et al. criteria when modest additional reddening ($A_V \leq 1.2$) is allowed, indicating that the extreme colors of these sources can be reproduced not only by obscured AGN, but by highly reddened star-formation as well. Indeed, when we include this star-forming template, as well as the star-forming LIRG/ULIRG templates of Rieke et al. (2008), the fraction of Fiore sources in our sample best-fit by a star-forming template rises from 20% to 66%.

The second argument for the Compton-thick nature of the Fiore et al. sources is the high fraction of heavily obscured AGN ($N_H = 10^{23} - 10^{26}$ cm $^{-2}$) required to reproduce the hardness ratios and counts of the stacked X-ray emission. Using a simulation, Fiore et al. (2007) estimate that 80% of their sources are obscured AGN. The prediction for the X-ray non-cataloged sources in our sample is somewhat lower: $60\%_{-40\%}^{+20\%}$, although this fraction rises for the weakly-detected IR-excess sources to $80\%_{-20\%}^{+10\%}$ (F. Fiore, private communication, 2008).

To test this finding for the sources in our sample, we coadded the 36 X-ray non-cataloged Fiore et al. sources that lie far enough from known X-ray sources to allow an accurate test for faint X-ray emission. The coaddition gave a soft detection (0.5-2 keV, 3.9σ), but only a weak hard detection (2-8 keV, 1.7σ). The resulting hardness ratio, $HR = (H - S)/(H + S) = -0.17$ is only slightly harder than that of the 10 X-ray cataloged Fiore et al. sources, $HR = -0.21$, whose column densities fall in the unobscured to highly obscured ($\log N_H$ (cm $^{-2}$) = 23.9) range (Tozzi et al. 2006), with a median value of $\log N_H$ (cm $^{-2}$) = 22.6).

If we stack only the 10 sources with weak X-ray counterparts (that also lie sufficiently far from known X-ray sources), however, we find a 5.3σ hard-band detec-

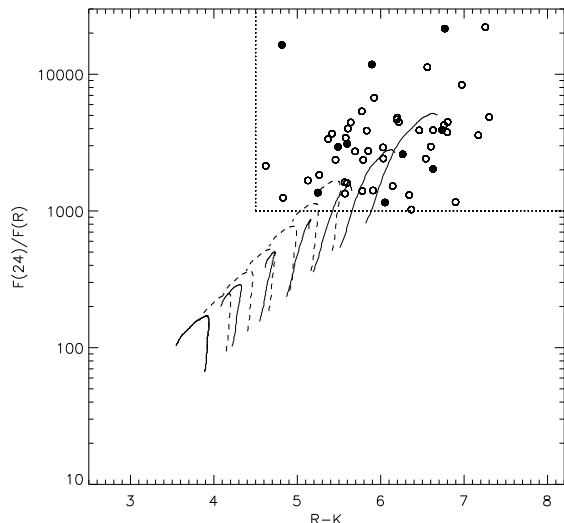


FIG. 13.— Redshifted ($z = 1.5 - 2.5$) tracks of the star-forming template IRAS 22491-1808 in Fiore et al. color space. Additional extinctions of $A_V = 0.0, 0.2, 0.4, 0.6, 0.8, 1.0$, and 1.2 were applied via the SMC (solid, Prevot et al. 1984, Bouchet et al. 1985) or Calzetti (dashed, Calzetti et al. 2000) extinction laws. The dotted lines represent the Fiore et al. (2008) selection criteria, and circles represent the 52 sources in our sample that meet those criteria. The 10 X-ray-detected sources are given as filled circles. The star-forming template enters the selection region with only a modest ($A_V \sim 1$) amount of additional extinction.

tion, a 4.7σ soft-band detection, and a hardness ratio of $HR = 0.33$, significantly harder than that of the X-ray cataloged sample. At a redshift of $z = 2$, this HR corresponds to a column density of $N_H = 2.7 \times 10^{23} \text{ cm}^{-2}$. The observed photon index, $\Gamma = 0.33$, indicates an obscured AGN origin, as it is inconsistent even with the moderately hard spectra of HMXB-dominated star-forming galaxies ($\Gamma \sim 1.0 - 1.4$). Stacking the remaining 26 X-ray-non-detected Fiore sources does not lead to a detection in any band. It therefore appears plausible, at least in this bright subset of the Fiore et al. sample, that the hard X-ray flux can be attributed to a small number of obscured, yet mostly Compton-thin, AGN, as opposed to a large number of obscured, Compton-thick AGN.

The third argument for the AGN nature of the Fiore et al. sources is the significant (factor of 30) offset between the IR and UV-derived SFRs. However, the inherent difficulties in determining accurate UV SFRs for luminous, heavily obscured galaxies (e.g. Goldader et al. 2002, Buat et al. 2005), as well as the systematic uncertainties of factors of 10-30 in the TIR luminosity (Fiore et al. 2008), make this the weakest of the 3 arguments.

Of the 52 Fiore et al. sources in our MIPS sample, 10 (19%) are therefore X-ray-selected AGN, and 10 (19%) are weakly detected in the X-ray, with coadded properties consistent with their being obscured AGN. As for the remaining 26 sources for which we can test for faint X-ray emission, we cannot rule out the presence of Compton-thick AGN. However, the lack of coadded hard counts from this X-ray non-detected sample, the significant fraction of such sources that can be fit by star-forming templates, and the Compton-thin nature of the X-ray-detected Fiore et al. sources all suggest that many of these sources, which make up the remaining 56% of the sample, are instead star-forming galaxies.

8. IMPLICATIONS FOR IR SELECTION OF AGN

Our evaluation of the performance of the infrared selection methods allows a preliminary estimate of the overall role of *Spitzer*-discovered AGN in the total population. Of the 109 X-ray sources in the MIPS-selected sample, 95 have redshifts, and of these, 73 (77%) have AGN-like X-ray luminosities of $(\log L_x(\text{ergs s}^{-1}) > 42)$. We therefore assume a sample of 84 (77% of 109) X-ray-selected AGN in the MIPS-selected sample. We now consider how many IR-selected AGN can be added to this total.

8.1. Infrared power-law and color-selected AGN

Of the 55 power-law AGN in our sample, 30 lack cataloged X-ray counterparts. If we assume that all of the X-ray weakly- and non-detected PLGs are AGN, the power-law selection criteria increases the number of known AGN (84) by 36%. Of the 25/30 X-ray non-cataloged sources for which we could test for faint emission, 7 (28%) show weak X-ray emission at the $> 2\sigma$ confidence level, and 18 show no sign of X-ray emission. Correcting for the 5 sources with nearby X-ray counterparts therefore gives an estimate of 8.4 weakly-detected sources. To place a conservative lower-limit on the contribution of X-ray non-detected PLGs to the AGN population, we select as AGN those PLGs that are either weakly-detected in the X-ray (8.4) or that have extremely red slopes of $\alpha < -1.0$ (8, see §6). Combining these two criteria results in a sample of 11.6 AGN candidates missed in the X-ray catalogs, for a contribution of 14%. We therefore conclude that PLG selection increases the number of known MIPS-detected AGN by $\sim 14 - 36\%$. Further adding the 3 color-selected galaxies that lie outside the 3σ star-forming contours and that lack cataloged X-ray counterparts (after correcting for the fraction with redshifts and for which the distance from the star-forming contours could therefore be determined) increases the contribution of IRAC-selected AGN to $\sim 18 - 40\%$.

A search for weak X-ray emission from the full sample of color-selected galaxies results in the detection of 44 additional sources, 70% of which have X-ray luminosities typical of AGN (see Table 2). Of these 30 AGN candidates, however, 19 (63%) lie at $z > 1.75$, the redshift above which nearly all (94%) MIPS sources meet the Lacy et al. criterion, regardless of their nature (AGN/star-forming). Their selection as AGN candidates is therefore not primarily a function of their IRAC colors, but of their X-ray properties. As such, we do not add these additional ~ 30 AGN candidates to our *Spitzer*-selected total.

8.2. Radio/Infrared-selected AGN

Radio/infrared selection, in which objects are selected for excess radio emission relative to that at $24 \mu\text{m}$, provides an alternative way to identify AGN independently of their optical and X-ray characteristics. In Donley et al. (2005), radio-excess AGN are defined as those sources with $\log f_{24 \mu\text{m}}/f_{1.4\text{GHz}} < 0$. Unlike PLGs, radio-excess AGN tend to lie at $z \sim 1$, have Seyfert-like X-ray luminosities of $\log L_x(\text{ergs s}^{-1}) \sim 42 - 43$, and have NIR SEDs dominated by the stellar bump (Donley et al. 2005). Of the PLGs detected in the CDF-N, only 3% meet the radio-excess criteria (Donley et al. 2007). While there is therefore almost no overlap between these two AGN

populations, their X-ray detection statistics are very similar: only 40% of radio-excess AGN are cataloged in the 2 Ms CDF-N. If we consider only those radio-excess AGN with $24\ \mu\text{m}$ flux densities in excess of $80\ \mu\text{Jy}$, the X-ray detection fraction rises to $\sim 60\%$. At this flux limit, the CDF-N sample is complete to radio-excess AGN as defined by Donley et al. (2005).

In the CDF-N, the X-ray and MIPS-detected radio-excess galaxies (with X-ray exposures greater than 1 Ms) account for 3% of the total number of such sources, and their X-ray non-detected counterparts increase the number of known AGN by 2%. Only 10-15% of AGN, however, are radio-intermediate or radio-loud. This small observed sample of radio-excess AGN is therefore indicative of an underlying population at least 7 times larger, which would increase the known population of MIPS-detected AGN by $\sim 15\%$ if a way could be found to identify them.

Martinez-Sansigre et al. (2006) also select high-redshift obscured AGN candidates via a $24\ \mu\text{m}$ and radio flux cut, although of the 21 AGN candidates chosen by them, only 6 (29%) are sufficiently radio loud to meet the infrared-to-radio selection criteria used above to define radio-excess AGN. Their selection, however, also includes a $3.6\ \mu\text{m}$ IRAC cut designed to select red galaxies. Because it is designed for use in shallow surveys, only three galaxies in the GOODS region of the CDF-N meet their MIPS and radio flux cuts (using the radio data of Richards 2000), and none are red enough to meet all three criteria. This selection method therefore does not contribute to the AGN sample in the deep CDF-S.

8.3. IR-excess Galaxies

As discussed above, the IR-excess samples of Daddi et al. (2007a), Dey et al. (2008), Polletta et al. (2008), and Fiore et al. (2008) contain various fractions of AGN and star-forming galaxies, with only the Polletta et al. selection criteria unquestionably identifying AGN. Of the Polletta et al. sources, however, 80% are detected in the X-ray catalogs, and the remaining source is a weakly-detected PLG, whose contribution to the AGN population has already been considered.

Daddi et al. (2007a,b) conclude that at least 50% of their IR-excess galaxies are Compton-thick AGN. If this hypothesis holds for the sources in our sample, the Daddi et al. selection criteria would contribute $\gtrsim 21$ AGN to the MIPS-selected sample in the ISAAC field, or $\gtrsim 31$ AGN to the full MIPS sample (as the ISAAC region comprises only 68% of our full survey area). As discussed in §7.1, however, it appears plausible that the properties of many of these sources can be attributed to star-formation. We therefore add only the weakly-detected galaxies, whose mean X-ray luminosity suggests a likely AGN origin. Of the 13 weakly-detected Daddi et al. IR-excess galaxies, 1 is a weakly-detected PLG and 1 is a color-selected galaxy that lies $> 3\sigma$ from the star-forming contours, leaving 11 sources whose contribution is yet to be counted (or 12.6 when we correct for the sources for which we could not test for weak X-ray emission). Further scaling to the full sample region results in an additional contribution of 18.6 sources, or 22%.

F. Fiore (private communication, 2008) likewise concludes that $\sim 60\%$ of the X-ray non-cataloged sources in our sample are obscured AGN. If so, our MIPS sample in

the ISAAC field should contain 25 X-ray weakly or non-detected Fiore-selected AGN. Of the 36/42 X-ray non-cataloged Fiore sources in our sample (which do not lie too close to a known X-ray source to test for faint emission), however, only 10 (28%) are X-ray weakly-detected (with properties indicative of heavy obscuration). The remaining 26 sources show no evidence for X-ray emission, and have properties that may also be consistent with star-formation. We therefore only consider the contribution from the 10 weakly-detected sources. Of these 10 sources, 3 are weakly-detected power-law galaxies. Correcting for the ISAAC field of view (and the 6 sources for which we could not test for weak X-ray emission) results in an additional contribution of 12.0 AGN, or 14%.

8.3.1. Combined Contribution

By combining the contribution of reliable power-law, color-selected, radio/infrared, and IR-excess AGN candidates, we therefore estimate that *Spitzer*-selected samples increase the known X-ray-selected AGN population by $\sim 54 - 77\%$, down to a $24\ \mu\text{m}$ flux density of $80\ \mu\text{Jy}$. In addition, the radio/infrared selection implies a $\sim 17\%$ contribution from radio-excess and radio-quiet AGN yet to be identified. The number of AGN with $24\ \mu\text{m}$ flux densities $> 80\ \mu\text{Jy}$ is therefore $71 - 94\%$ larger than that of current samples detected both in the X-ray and at $24\ \mu\text{m}$ in the deepest X-ray fields.

9. AGN FRACTION OF THE MIR SAMPLE

We plot in Figure 14a the fraction of the MIPS sample comprised of MIR-dominated AGN as a function of $24\ \mu\text{m}$ flux density. We define as 'MIR-dominated' those AGN that (1) meet the PLG criteria, provided that they are also X-ray-weakly-detected or have extremely red slopes of $\alpha < -1.0$ (these criteria were used above to place a conservative lower limit on the contribution from PLGs), (2) meet the IRAC color-color cuts of Lacy et al. (2004) or Stern et al. (2005) and lie outside the 3σ star-forming contours, (3) meet the Polletta et al. (2008) criteria, (4) meet the Fiore et al. (2008) criteria and are X-ray cataloged or weakly-detected, or (5) meet the Daddi et al. (2007) criteria and are X-ray cataloged or weakly-detected. As above, we define as X-ray AGN those sources with cataloged X-ray counterparts whose total X-ray luminosities (when redshifts are available) exceed $10^{42}\ \text{ergs s}^{-1}$. Because the PLG, Daddi et al. (2007), and Fiore et al. (2008) selection criteria all identify AGN candidates with mean redshifts of $z \sim 2$, the vast majority of the IR-selected AGN lie at high redshift regardless of their flux density.

As shown by Brand et al. (2006), the fraction of MIR sources dominated by an AGN drops with decreasing flux density. We verify this trend, showing excellent agreement with the Brand et al. results (see Figure 13a), and confirm that it continues down to $\sim 300\ \mu\text{Jy}$. At lower flux densities, however, the fraction of MIR-dominated X-ray AGN begins to decrease at a much lower rate, and that of all MIR-dominated AGN plateaus at a value of $\sim 10\%$. This indicates that a non-negligible fraction of faint MIR sources are not powered primarily by star-formation, but by their central engines. The significant number of faint $24\ \mu\text{m}$ sources that are AGN-dominated in the MIR is consistent with the finding of 6/19 such objects in the spectroscopy of faint $24\ \mu\text{m}$ sources by

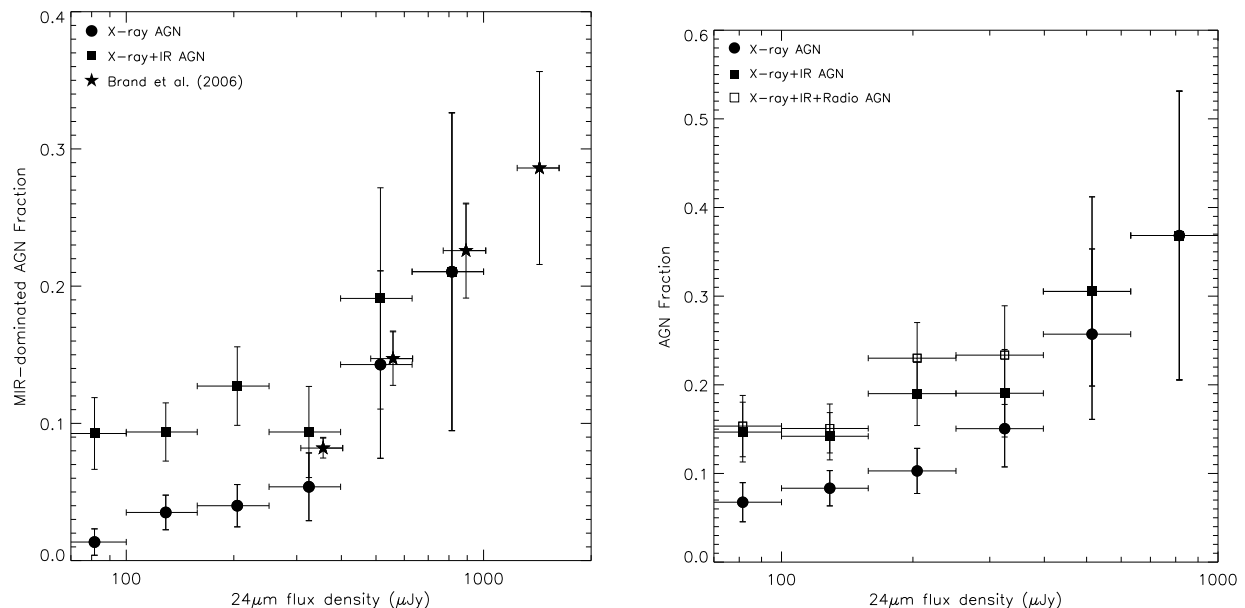


FIG. 14.— Fraction of MIR-dominated AGN, and all AGN (regardless of their contribution to the MIR light), as a function of $24\ \mu\text{m}$ flux density. The full definitions of ‘MIR-dominated’ and ‘X-ray AGN’ are given in §9. Error bars represent the 1σ errors on the source number counts, and the width of the bins. The MIR-selected sources missed in the X-ray comprise the majority of the MIR-dominated AGN at low flux densities, where the trend towards lower AGN fractions plateaus.

Rigby et al. (2008). At these low flux densities, it is also evident from Figure 14a that the majority of the MIR-dominated AGN are not detected in the X-ray. For instance, at $80\ \mu\text{Jy}$, the total number of MIR-dominated AGN outnumbers that of MIR-dominated X-ray AGN by a factor of ~ 6 . Using only the X-ray emission as a probe of AGN activity will therefore result in a serious underestimation of the AGN contribution to the MIR flux density.

Finally, we plot in Figure 14b the fraction of all AGN in the MIPS sample (not only those whose MIR flux is dominated by the AGN), as a function of MIPS $24\ \mu\text{m}$ flux density. To account for the contribution of the AGN amongst the 14 X-ray sources lacking redshifts, we randomly add 11, or 77% (the AGN fraction of the X-ray sample), of these 14 X-ray sources to the X-ray AGN sample. We further supplement the AGN sample by including the assumed contribution from radio-excess and radio-quiet AGN, 17%, or 14 sources. Because these sources have not been individually identified in the CDF-S, we draw their flux densities randomly from the range of observed flux densities in the CDF-N ($80 - 300\ \mu\text{Jy}$).

The X-ray non-detected AGN still comprise the majority of all AGN at the lowest $24\ \mu\text{m}$ flux densities, and their contribution at larger flux densities is significant, raising the AGN fraction to $> 15\%$ at all $24\ \mu\text{m}$ flux densities. As was seen for the MIR-dominated AGN, the total fraction of AGN rises with increasing MIR flux density, reaching a value of 37% at $f_{24\ \mu\text{m}} \sim 800\ \mu\text{Jy}$, 15% higher than that of MIR-dominated AGN of the same flux density. The X-ray AGN fractions we find are somewhat higher than that of Treister et al. (2006). While the cause of this offset is not entirely clear, it is likely to be due at least in part to cosmic variance, as their $24\ \mu\text{m}$ sample was drawn from GOODS-N, and ours from GOODS-S. Once again, the vast majority of X-ray non-detected AGN at all flux densities lie at $z \sim 2$, the mean redshift of the sources selected via the PLG, Daddi et

al. (2007), and Fiore et al. (2008) criteria. Only the radio-selected AGN samples lie at systematically lower redshifts of $z \sim 1$.

10. SUMMARY

Infrared selection of AGN is a powerful technique. Using new accurate star-forming and AGN templates along with a flux-limited MIPS-selected sample drawn from the GOODS-S field, we critically review three MIR selection criteria: (1) the IRAC color cuts of Lacy et al. (2004) and Stern et al. (2005), (2) the power-law galaxy (PLG) selection technique of Alonso-Herrero et al. (2006) and Donley et al. (2007), and (3) the IR-excess selection criteria of Daddi et al. (2007a,b), Dey et al. (2008), Fiore et al. (2008), and Polletta et al. (2008). From this analysis, we then quantify the contribution of *Spitzer*-selected AGN to the X-ray selected AGN population. The main conclusions of this paper are as follows:

- The majority of non-power-law IRAC color-selected AGN candidates have IR colors consistent with those of redshift-appropriate star-forming templates. In comparison, the majority of PLG AGN candidates lie outside of the star-forming contours. PLG selection recovers the majority of high-quality AGN candidates.
- The reliability of AGN IRAC color-color selection improves with increasing flux as high-redshift star-forming galaxies fall out of the sample. Nevertheless, the fraction of potential star-forming contaminants is still high ($\sim 50\%$) at the highest fluxes probed by our survey ($f_{24\ \mu\text{m}} \sim 500\ \mu\text{Jy}$).
- A comparison of the $24\ \mu\text{m}$ to $3.6\ \mu\text{m}$ colors of the X-ray non-detected PLGs to those of AGN and star-forming templates suggests that the X-ray non-detected PLGs, like their X-ray-detected counterparts, have more hot dust emission than can be explained by star-formation alone.

- An analysis of the Daddi et al. (2007) IR-excess sources in our MIPS sample indicates that while these sources may be Compton-thick AGN, it is also possible that they are low-luminosity, Compton-thin AGN and/or luminous, highly-reddened star-forming galaxies.
- An X-ray stacking analysis of the sources selected via the Fiore et al. (2008) criteria indicate that $\sim 42\%$ of the sources are consistent with being obscured AGN, and that the remaining 58% may be star-forming galaxies.
- Adding secure *Spitzer*-selected power-law, color-color, radio/IR, and IR-excess AGN candidates to the deepest X-ray samples directly increases the number of known AGN by $\sim 54 - 77\%$, and implies a total increase of $71 - 94\%$. This fraction excludes the full contributions from the Daddi et al. and Fiore et al. AGN candidates, whose nature is still uncertain.
- The fraction of MIR sources dominated by an AGN decreases with decreasing flux density, but only down to a $24\ \mu\text{m}$ flux density of $\sim 300\ \mu\text{Jy}$. Below this limit, the AGN fraction levels out at $\sim 10\%$. This indicates that a non-negligible fraction of faint $24\ \mu\text{m}$ sources are primarily powered not by star-formation, but by the central engine. In addition, the majority of AGN at low $24\ \mu\text{m}$ flux densities are missed in the X-ray, indicating that X-ray emission alone cannot be used to identify AGN, especially amongst faint IR samples.

We thank M. Polletta for providing templates, M. Dickinson, and D. Alexander for providing the list of Daddi et al. (2007a,b) sources. We also thank D. Alexander, F. Fiore, M. Lacy, D. Stern, and the anonymous referee for discussions and comments that improved the paper. Finally, we thank Caltech/JPL for support through contract 1255094 to the University of Arizona. P. G. P.-G. acknowledges support from the Spanish Programa Nacional de Astronomía y Astrofísica under grant AYA 2006-02358 and AYA 2006-15698-C02-02, and from the Ramón y Cajal Program financed by the Spanish Government and the European Union.

REFERENCES

- Alexander, D. M., Vignali, C., Bauer, F. E., Brandt, W. N., Hornschemeier, A. E., Garmire, G. P., & Schneider, D. P. 2002, *AJ*, 123, 1149
- Alexander, D. M., et al. 2003, *AJ*, 126, 539
- Alexander, D. M., et al. 2008, *ArXiv e-prints*, 803, arXiv:0803.0636
- Alonso-Herrero, A., et al. 2006, *ApJ*, 640, 167
- Arnouts, S., Vandame, B., Benoist, C., Groenewegen, M. A. T., da Costa, L., Schirmer, M., Mignani, R. P., & Slikhuis, R. 2002, *VizieR Online Data Catalog*, 337, 90740
- Barmby, P., et al. 2006, *ApJ*, 642, 126
- Bevington, P. R., & Robinson, D. K. 2003, *Data reduction and error analysis for the physical sciences*, 3rd ed., by Philip R. Bevington, and Keith D. Robinson. Boston, MA: McGraw-Hill, ISBN 0-07-247227-8, 2003.
- Bolzonella, M., Miralles, J.-M., & Pelló, R. 2000, *A&A*, 363, 476
- Bouchet, P., Lequeux, J., Maurice, E., Prevot, L., & Prevot-Burnichon, M. L. 1985, *A&A*, 149, 330
- Brand, K., et al. 2006, *ApJ*, 644, 143
- Brusa, M., et al. 2005, *A&A*, 432, 69
- Buat, V., et al. 2005, *ApJ*, 619, L51
- Calzetti, D., Armus, L., Bohlin, R. C., Kinney, A. L., Koornneef, J., & Storchi-Bergmann, T. 2000, *ApJ*, 533, 682
- Calzetti, D., et al. 2007, *ApJ*, 666, 870
- Caputi, K. I., et al. 2006, *ApJ*, 637, 727
- Cardamone, C. N., et al. 2008, *ApJ*, 680, 130
- Daddi, E., et al. 2007a, *ApJ*, 670, 156
- Daddi, E., et al. 2007b, *ApJ*, 670, 173
- Dale, D. A., & Helou, G. 2002, *ApJ*, 576, 159
- Desai, V., et al. 2008, *ApJ*, 679, 1204
- Dey, A., et al. 2008, *ApJ*, 677, 943
- Doherty, M., Bunker, A. J., Ellis, R. S., & McCarthy, P. J. 2005, *MNRAS*, 361, 525
- Donley, J. L., Rieke, G. H., Rigby, J. R., & Pérez-González, P. G. 2005, *ApJ*, 634, 169
- Donley, J. L., Rieke, G. H., Pérez-González, P. G., Rigby, J. R., & Alonso-Herrero, A. 2007, *ApJ*, 660, 167
- Elvis, M., et al. 1994, *ApJS*, 95, 1
- Fazio, G. G., et al. 2004, *ApJS*, 154, 10
- Ferrarese, L., & Merritt, D. 2000, *ApJ*, 539, L9
- Fiore, F., et al. 2008, *ApJ*, 672, 94
- Franceschini, A., et al. 2003, *MNRAS*, 343, 1181
- Gebhardt, K., et al. 2000, *ApJ*, 539, L13
- Genzel, R., et al. 1998, *ApJ*, 498, 579
- Giacconi, R., et al. 2002, *ApJS*, 139, 369
- Giavalisco, M., et al. 2004, *ApJ*, 600, L93
- Gilli, R., Comastri, A., & Hasinger, G. 2007, *A&A*, 463, 79
- Goldader, J. D., Meurer, G., Heckman, T. M., Seibert, M., Sanders, D. B., Calzetti, D., & Steidel, C. C. 2002, *ApJ*, 568, 651
- Grazian, A., et al. 2006, *A&A*, 449, 951
- Hopkins, P. F., Hernquist, L., Cox, T. J., Di Matteo, T., Robertson, B., & Springel, V. 2006, *ApJS*, 163, 1
- Ivezić, Ž., et al. 2002, *AJ*, 124, 2364
- Iwasawa, K., Matt, G., Guainazzi, M., & Fabian, A. C. 2001, *MNRAS*, 326, 894
- Kennicutt, R. C., Jr. 1998, *ApJ*, 498, 541
- Klaas, U., et al. 2001, *A&A*, 379, 823
- Klesman, A., & Sarajedini, V. 2007, *ApJ*, 665, 225
- Lacy, M., et al. 2004, *ApJS*, 154, 166
- Lacy, M., et al. 2005, *ApJS*, 161, 41
- Lacy, M., Petric, A. O., Sajina, A., Canalizo, G., Storrie-Lombardi, L. J., Armus, L., Fadda, D., & Marleau, F. R. 2007, *AJ*, 133, 186
- Le Fèvre, O., et al. 2004, *A&A*, 428, 1043
- Lonsdale, C. J., et al. 2003, *PASP*, 115, 897
- Martínez-Sansigre, A., Rawlings, S., Lacy, M., Fadda, D., Jarvis, M. J., Marleau, F. R., Simpson, C., & Willott, C. J. 2006, *MNRAS*, 370, 1479
- Marzke, R., et al. 1999, *Photometric Redshifts and the Detection of High Redshift Galaxies*, 191, 148
- McGregor, P. J. 1987, *ApJ*, 312, 195
- Mignoli, M., et al. 2005, *A&A*, 437, 883
- Neugebauer, G., Oke, J. B., Becklin, E. E., & Matthews, K. 1979, *ApJ*, 230, 79
- Pérez-González, P. G., et al. 2005, *ApJ*, 630, 82
- Pérez-González et al. 2008, *ApJ*, in press
- Persic, M., & Rephaeli, Y. 2002, *A&A*, 382, 843
- Persic, M., Rephaeli, Y., Braito, V., Cappi, M., Della Ceca, R., Franceschini, A., & Gruber, D. E. 2004, *A&A*, 419, 849
- Polletta, M., et al. 2007, *ApJ*, 663, 81
- Polletta, M., Weedman, D., Hönig, S., Lonsdale, C. J., Smith, H. E., & Houck, J. 2008, *ApJ*, 675, 960
- Pozzi, F., et al. 2007, *A&A*, 468, 603
- Prevot, M. L., Lequeux, J., Prevot, L., Maurice, E., & Rocca-Volmerange, B. 1984, *A&A*, 132, 389
- Ptak, A., Heckman, T., Levenson, N. A., Weaver, K., & Strickland, D. 2003, *ApJ*, 592, 782
- Ranalli, P., Comastri, A., & Setti, G. 2003, *A&A*, 399, 39
- Richards, E. A. 2000, *ApJ*, 533, 611
- Richards, G. T., et al. 2003, *AJ*, 126, 1131
- Rieke, G. H., et al. 2004, *ApJS*, 154, 25
- Rieke, G. H., et al. 2008, in prep.
- Rigby, J. R., et al. 2004, *ApJS*, 154, 160
- Rigby, J. R., et al. 2008, *ApJ*, 675, 262
- Sajina, A., Lacy, M., & Scott, D. 2005, *ApJ*, 621, 256
- Sanders, D. B., Mazzarella, J. M., Kim, D.-C., Surace, J. A., & Soifer, B. T. 2003, *AJ*, 126, 1607
- Silva, L., Granato, G. L., Bressan, A., & Danese, L. 1998, *ApJ*, 509, 103
- Steffen, A. T., Brandt, W. N., Alexander, D. M., Gallagher, S. C., & Lehmer, B. D. 2007, *ApJ*, 667, L25
- Stern, D., et al. 2005, *ApJ*, 631, 163
- Szokoly, G. P., et al. 2004, *ApJS*, 155, 271
- Teng, S. H., Wilson, A. S., Veilleux, S., Young, A. J., Sanders, D. B., & Nagar, N. M. 2005, *ApJ*, 633, 664
- Tozzi, P., et al. 2006, *A&A*, 451, 457
- Treister, E., et al. 2006, *ApJ*, 640, 603
- Vandame, B., et al. 2001, *ArXiv Astrophysics e-prints*, arXiv:astro-ph/0102300
- Vanzella, E., et al. 2006, *A&A*, 454, 423
- Vijh, U. P., Witt, A. N., & Gordon, K. D. 2003, *ApJ*, 587, 533
- White, N. E., Swank, J. H., & Holt, S. S. 1983, *ApJ*, 270, 711
- Wolf, C., et al. 2004, *A&A*, 421, 913
- Yan, L., et al. 2007, *ApJ*, 658, 778

TABLE 1
PHOTOMETRIC REDSHIFTS

Sample	N _{srcs}	N _z	N _{spec}	Δz	σ_z	% with $\Delta z > 0.10$	% with $\Delta z > 0.20$
All	713	649	249	0.012	0.15	11.3%	4.6%
IR-Normal	448	424	187	0.012	0.12	7.2%	2.8%
Color-Selected	210	196	51	0.015	0.10	20.4%	4.1%
Power-law	55	29	11	-0.013	0.48	40.0%	40.0%

TABLE 2
X-RAY DETECTION STATISTICS

	MIPSA ^a Sample	MIPS/ISAAC Sample	Daddi et al. (2007)	Dey et al. (2008)	Fiore et al. (2008)	Polletta et al. (2008)	$f_{24} \mu\text{m}/f_R$ > 1000	All IR-Excess
Total	713	465	42	10	52	5	71	101
X-rays	109	76	3	3	10	4	11	15
Power	25 (100%)	14	0	3	4	4	4	7
Color	35 (79%)	28	3	0	5	0	6	7
Normal	49 (65%)	34	0	0	1	0	1	1
Weak X-rays	157	125	13	2	10	1	16	26
Power	7 (100%)	5	1	1	3	1	4	4
Color	44 (70%)	35	11	1	7	0	11	20
Normal	106 (19%)	85	1	0	0	0	1	2
No X-rays	361	226	21	3	26	0	38	51
Power	18	12	3	0	7	0	9	11
Color	109	72	15	3	19	0	28	36
Normal	234	142	3	0	0	0	1	4

NOTE. — The sum of the weakly and non-detected sources does not equal the full number of X-ray non-cataloged sources. The difference represents the number of sources that lie too close to a known X-ray counterpart to test for faint X-ray emission.

^a The fraction of X-ray sources with AGN X-ray luminosities of $\log L_X(\text{ergs s}^{-1}) > 42$ is given in parentheses.

TABLE 3
FRACTION OF SOURCES THAT LIE OUTSIDE THE
STAR-FORMING CONTOURS

Selection	1σ	2σ	3σ
Lacy	52%	21%	10%
Stern	40%	18%	8%
Power-law	93%,82%	79%,61%	71%,43%
Lacy	29%	12%	5%
Stern	22%	5%	0%
Power-law	71%,68%	61%,46%	57%,39%

NOTE. — The upper portion of the table assumes no errors on the photometric redshifts. The lower portion assumes 10% errors. The two values given for the PLGs represent the fraction of sources that lie outside the star-forming contours in Lacy and Stern color-space, respectively.

APPENDIX

APPENDIX A: PHOTOMETRIC REDSHIFT TECHNIQUES

We used two methods to determine photometric redshifts. The first utilizes the extensive high-resolution template set of Pérez-González et al. (2008), which was created by fitting stellar population synthesis and dust emission models to the ~ 1500 galaxies in the CDF-N and CDF-S with secure spectroscopic redshifts. When applied to all spectroscopically-detected IRAC-selected galaxies in the GOODS-N and GOODS-S, this template library returns photometric redshifts with $\Delta(z) < 0.1$ for 88% of the sources, and $\Delta(z) < 0.2$ for 96%, where $\Delta(z) = (z_p - z_s)/(1 + z_s)$ (Pérez-González et al. 2008). Because this method relies on star-forming templates, however, we do not expect it to provide equally reliable photometric redshifts for galaxies in which the stellar features are dominated by emission from an AGN.

Our second method is based on the chi-squared minimization routine HYPERZ (Bolzonella, Miralles, & Pelló 2000). With a suite of normal star-forming, LIRG/ULIRG, and AGN templates, we can better account for the range of sources

TABLE 4
X-RAY DETECTION FRACTION (AND TOTAL NUMBER) OF
SOURCES THAT LIE OUTSIDE THE STAR-FORMING CONTOURS

Selection	1σ		2σ		3σ	
Lacy	21%	(19)	26%	(10)	42%	(8)
Power-law (Lacy)	70%	(19)	83%	(19)	90%	(19)
Stern	19%	(5)	25%	(3)	40%	(2)
Power-law (Stern)	67%	(16)	72%	(13)	85%	(11)
Lacy	29%	(15)	36%	(8)	67%	(6)
Power-law (Lacy)	81%	(17)	89%	(16)	88%	(15)
Stern	14%	(2)	0%	(0)	0%	(0)
Power-law (Stern)	80%	(16)	86%	(12)	82%	(9)

NOTE. — The upper portion of the table assumes no errors on the photometric redshifts. The lower portion assumes 10% errors.

TABLE 5
PERCENT OF SECURE COLOR-SELECTED
GALAXIES VS. $24\ \mu\text{m}$ FLUX

$24\ \mu\text{m}$ flux cut (μJy)	Lacy	Stern	Power-law
80	52%	40%	93%, 82%
100	54%	44%	96%, 84%
150	53%	43%	94%, 78%
200	60%	63%	100%, 76%
300	53%	25%	100%, 72%
400	52%	50%	100%, 66%
500	56%	50%	100%, 71%
80	29%	21%	72%, 68%
100	29%	24%	76%, 72%
150	25%	21%	73%, 63%
200	32%	27%	92%, 76%
300	31%	25%	90%, 72%
400	39%	50%	88%, 66%
500	50%	50%	85%, 71%

NOTE. — The upper portion of the table assumes no errors on the photometric redshifts. The lower portion assumes 10% errors. The two values given for the PLGs represent the fraction of sources that lie outside the star-forming contours in Lacy and Stern color-space, respectively.

expected in our $24\ \mu\text{m}$ selected sample, albeit with a smaller template library. To create this library, we started with a sample of 10 star-forming templates and 8 AGN templates from Silva et al. (1998) and Polletta et al. (2007). The Polletta et al. AGN templates cover a range of intrinsic obscurations (Type 1 and Type 2) and luminosities (Sey/QSO). We then supplemented this sample with 10 empirical star-forming LIRG and ULIRG templates. The full template sample is listed in Table 1. The LIRG and ULIRG templates, described in detail in Rieke et al. (2008, in prep.), significantly improve upon previous semi-empirical templates by constraining the SEDs between 1 and $6\ \mu\text{m}$ with 2MASS and IRAC photometry and by basing the SEDs from 5 to $35\ \mu\text{m}$ on IRS spectra.

Using this template library, we ran HYPERZ on all robust optical-MIR data for the IR-normal and color-selected galaxies. For the PLGs, we removed all photometry longward of $3.6\ \mu\text{m}$ (IRAC channel 1). Including the full *Spitzer* photometry for PLGs provided little or no additional constraint on potential redshifts, and limited severely the SEDs for which a good fit could be found. We allowed z to vary from 0 to 4 and A_v to vary from 0 to 1.2. While its shape is still relatively unconstrained, a number of studies have suggested that the extinction curve of AGN most closely resembles that of the SMC (e.g. Richards et al. 2003). We therefore assumed by default the SMC extinction curve of Bouchet et al. (1985) for the PLGs and color-selected galaxies. For the IR-normal galaxies, we assume the Calzetti (2000) extinction curve, as this curve was modeled to represent the extinction properties of starburst galaxies. To prevent unrealistic redshift solutions, we applied the redshift- and model-dependent absolute magnitude cuts of Polletta et al. (2007). Finally, to increase the weight of the IRAC photometry, which solely defines the red slope of the stellar bump, we set the errors on the IRAC photometry to the measurement errors, as opposed to the total photometric errors. This procedure is acceptable because many types of photometric error will have similar effects on the four IRAC bands, so we are making use of the overall internal consistency expected for the data.

TABLE 1
A1: PHOTOMETRIC REDSHIFT TEMPLATES

Template	Type	Ref
Ell2	2 Gyr old elliptical	(2)
Ell5	5 Gyr old elliptical	(2)
Ell13	13 Gyr old elliptical	(2)
S0	Spiral 0	(1)
Sa	Spiral a	(1)
Sb	Spiral b	(1)
Sc	Spiral c	(1)
Sd	Spiral d	(1)
Sdm	Spiral dm	(1)
M82	Starburst	(1)
NGC 6090	LIRG/Starburst	(1)
ESO320-G030	LIRG/Starburst	(3)
NGC 1614	LIRG/Starburst	(3)
NGC 2639	LIRG/Starburst	(3)
NGC 3256	LIRG/Starburst	(3)
NGC 4194	LIRG/Starburst	(3)
Arp 220	ULIRG/Starburst	(1)
Arp 220	ULIRG/Starburst	(3)
IRAS 12112+0305	ULIRG/Starburst	(3)
IRAS 14348-1447	ULIRG/Starburst	(3)
IRAS 17208-0014	ULIRG/Starburst	(3)
IRAS 22491-1808	ULIRG/Starburst	(3)
IRAS 22491-1808	ULIRG/Starburst	(1)
Mrk 231	ULIRG/Seyfert 1	(1)
Sey1.8	Seyfert 1.8	(1)
TQSO1	Type 1 QSO	(1)
Sey2	Seyfert 2	(1)
NGC 6240	Starburst/Seyfert 2	(1)
IRAS 19254-7245	ULIRG/Seyfert 2	(1)
IRAS 20551-4250	ULIRG/Buried AGN	(1)
QSO2	Type 2 QSO	(1)

REFERENCES. — (1) Polletta et al. (2007), (2) Silva et al. (1998), (3) Rieke et al. (2008)

To improve the likelihood of obtaining a good fit for each source, we then varied a number of these assumptions, and examined by eye the resulting fits to choose the most convincing redshift solution. This visual inspection is an important characteristic of our work, and was made possible by the relatively small number of sources in our sample. First, each PLG and color-selected galaxy was fit by both the SMC and Calzetti extinction laws. In most cases, the resulting redshift fits and solutions varied only slightly (in which case we chose the SMC-derived fit), but for some galaxies, one of the two extinction laws provided a clearly superior fit as determined by a visual inspection. Second, if the absolute magnitude of the resulting best-fit template did not meet the redshift-dependent absolute magnitude cut of Polletta et al. (2007), we allowed M_B to vary between -23.7 to -17 for star-forming templates and -28.8 to -19 for AGN templates (e.g. Polletta et al. 2007). Third, we allowed the IRAC errors to increase to their total estimated values by adding a 10% error to the flux; in only 4 cases did this lead to a better fit. Finally, for the PLGs, we explored fits that did not include the 3.6 μm IRAC channel; only 2 sources benefited from this change.

The final step in our redshift estimation was an independent review of the redshifts by two authors. By examining by eye the resulting redshift fits, we chose for each PLG and color-selected galaxy the best HYPERZ redshift. We then compared this to the redshift fit from the Pérez-González et al. (2008) technique, and replaced the former with the latter if it clearly provided a better fit. For the IR-normal galaxies, we use the Pérez-González et al. (2008) redshifts by default, as these are optimized for normal galaxies. We do, however, remove unconvincing redshift fits, and substitute a solid HYPERZ redshift if available. For all sources, we only assign a photometric redshift if a convincing fit exists. We rejected 76 sources with poor data or other problems that compromise our redshift determination. The photometric redshifts classified as being of high quality are summarized in Table 1 and shown in Figure 1.

APPENDIX B: REDSHIFT-DEPENDENT COLOR SELECTION

$$z = 0 - 0.25$$

The lowest redshift bin contains no PLGs and 2 color-selected galaxies, both of which are detected in the X-ray, but with low observed X-ray luminosities of $\log L_x(\text{ergs s}^{-1}) = 41.3$ and $\log L_x(\text{ergs s}^{-1}) = 40.9$, indicative of powerful starbursts or very low-luminosity AGN.

$$z = 0.25 - 0.75$$

The second redshift bin contains 3 PLGs, 27 Lacy-selected galaxies, and 4 Stern-selected galaxies. Of the Lacy and Stern-selected sources, only 41% and 25% are detected in the X-ray, respectively, compared to 100% of the PLGs. The average observed 0.5-8 keV X-ray luminosity of the X-ray-detected color-selected galaxies, $\log L_x(\text{ergs s}^{-1}) =$

43.0, is consistent with AGN activity, but is an order of magnitude less than that of the PLGs in this redshift bin, $\log L_x(\text{ergs s}^{-1}) = 44.1$. This is not surprising, as power-law selection preferentially identifies the most luminous AGN where the emission from the central engine is able to overpower that of the host galaxy (Donley et al. 2007). The AGN that lie amongst the color-selected sample clearly represent a less luminous AGN population than those selected via the PLG criteria. Furthermore, of the 27 Lacy-selected (and 4 Stern-selected) galaxies, only 11 (2) lie outside the 1σ star-forming contours in their respective color-space, with the number dropping to 3 and 1 (2 and 0) at 2σ and 3σ . This suggests that the majority of the color-selected sources in this redshift bin have infrared colors indicative of IR-normal galaxies. While all of the PLGs lie outside even the 3σ contours in the Lacy color-space, they lie inside the contours in Stern-space, due primarily to the Sdm template of Polletta et al. (2007), whose strong $3.3 \mu\text{m}$ aromatic feature passes through the $4.5 \mu\text{m}$ IRAC band at $z \sim 0.4$, causing the template to enter the Stern AGN selection region at $z = 0.23 - 0.51$. Of the 2 PLGs whose colors overlap with this template, both have spectroscopic redshifts of $z > 0.67$, and would therefore be 'safe' if we considered smaller redshift bins. Removing this template, however, would have no effect on the number of Lacy or Stern-selected sources that lie outside the 1σ contours.

$$z = 0.75 - 1.25$$

We find a higher proportion of secure color-selected galaxies in the $z = 0.75 - 1.25$ bin, with 10/12 of the Lacy-selected sources and 6/13 of the Stern-selected sources lying outside the 1σ star-forming contours. This is not surprising, as it is at $z \sim 1$ that the star-forming contours are best separated from the AGN selection region. If we extend our test to 2σ , however, the numbers drop significantly, to 5/12 and 1/13. The majority of the Stern-selected galaxies in this redshift bin fill the lower-left corner of the AGN selection region, the region populated by the Stern-only sources whose Lacy colors place them in the star-forming locus of color-space. These star-forming galaxies are likely responsible for the fact that this is the only redshift bin in which the Stern-selected sources outnumber the Lacy-selected sources. Of the 5 PLGs in this redshift bin, all lie outside the 1σ star-forming contours in both Lacy and Stern color-space, and while only 3 lie outside of the 2σ contours in Stern color-space, all lie outside of the 2σ and 3σ colors in Lacy color-space.

$$z = 1.25 - 1.75$$

The number of color-selected galaxies rises significantly in the $z = 1.25 - 1.75$ redshift bin. The fraction of potential IR-selected AGN, however, is by far the lowest at these redshifts, with only 6/38 Lacy-selected sources and 3/31 Stern-selected sources falling outside the 1σ star-forming contours. In addition, only 3/38 Lacy sources and 4/31 Stern sources have X-ray counterparts, further suggesting that nearly all of the color-selected sources at this redshift are star-forming galaxies, and not AGN. In contrast, the 2 PLGs found in this redshift bin fall outside of the 1σ contours in both the Lacy and Stern plots, and both are detected in the X-ray.

$$z = 1.75 - 2.25$$

The largest number of Lacy-selected sources, 77, is found in the $z = 1.75 - 2.25$ bin. In addition, an extraordinarily high fraction, 50/77, lie outside of the 1σ star-forming contours, a surprising fact given the X-ray detection fraction of only 9%. Have we discovered a significant population of $z \sim 2$ obscured AGN similar to those claimed by Daddi et al. (2007), or is there another explanation for this population?

The AGN contours (shown in green) provide a better match to the IR colors of these color-selected galaxies than do the star-forming templates (shown in blue). At this redshift, the primary difference between the IRAC regions of the star-forming and the low-luminosity AGN templates is the strength of the CO index, which is stronger in the star-forming galaxies than in the AGN. The MIPS-selected sources therefore may have smaller CO indices than those of our local templates. One explanation for this offset is that an underlying AGN continuum has diluted this feature. A lower CO index, however, could also be attributed to evolution in the metallicity of the LIRGS/ULIRGS. At 1/3 solar metallicity, the CO index drops by 4-6 percentage points (McGregor 1987), causing the contours to shift upwards in Lacy color space by ~ 0.08 . While this lessens this offset between the colors of star-forming contours and the observed galaxies, it cannot fully account for the observed discrepancy. Thus, if a change in the CO index is invoked for the offset, it is likely that AGN continua are also present.

However, other possible explanations exist. If we incorporate into the contours a 10% error in $(1+z)$ (recall that the measured σ for our photometric redshift fits was 0.15 and that 11% of the sources in our spectroscopic redshift sample have photometric errors $> 10\%$) the resulting contours are far-better matched to the IR-colors of the color-selected galaxies. Of the Lacy- and Stern-selected galaxies, only 17% and 9% now lie outside of the 1σ contours, with the numbers dropping to 8% and 0% at 2σ and 4% and 0% at 3σ , respectively.

The templates with which the photometric redshifts were best fit can provide further insight into the sources in this redshift bin. Of the 90 non-PLGs in the $z \sim 2$ bin, 75 (86%) are best fit by a star-forming ULIRG template, 9 (10%) are best fit by a ULIRG/hidden AGN template, 1 (1%) is best-fit by a type 2 AGN template, and 1 (1%) is best fit by a type 1 AGN template. In contrast, all of the PLGs in this redshift range are best-fit by a type 2 AGN template. Therefore, while we can not rule out the possibility that we have detected a sample of high-redshift, heavily obscured AGN, the extremely low X-ray detection fraction of 9%, the much improved fit of the contours for which 10% errors in the photometric redshifts were included, and the overwhelming fraction of sources for which a purely star-forming ULIRG provided the best fit to the SED suggest that it is more likely that the vast majority of color-selected galaxies in this redshift bin are star-forming galaxies, not AGN.

$z > 2.25$

The number of color-selected galaxies in the remaining two redshift bins is relatively low: 18 Lacy-selected sources and 5 Stern selected sources. Of these, a large fraction (61% and 80%, respectively) lie outside of the star-forming contours, which cover a comparatively small portion of the color-space. At 2σ and 3σ , the fractions drop to 39% and 11% (Lacy) and 20% and 0% (Stern). At these redshifts, the X-ray detection fractions of both the color-selected sources and the PLGs are low: 17% for the Lacy sources, 40% for the Stern sources, and 23% for the PLGs. At $z = 2.5$, an unobscured AGN with $\Gamma = 2$ requires a rest-frame 0.5-8 keV luminosity of $\log L_x(\text{ergs s}^{-1}) = 42.8$ to meet the flux limit within $1'$ of the CDF-S aimpoint. At $z = 3$, the required value rises to $\log L_x(\text{ergs s}^{-1}) = 43.0$, suggesting that if these sources are AGN, they must have low luminosities, or high obscuring columns.

$z = \text{unknown}$

Not all sources in our sample have redshift estimates. The redshift completeness for the Lacy and Stern color-selected samples is high (93% and 90%, respectively), but we have high-quality redshifts for only 49% of the PLGs. The difficulty in fitting redshifts to these sources stems largely from their faint fluxes: the power-law (color-selected) galaxies without redshifts are significantly fainter, $V = 26.2$ (25.3), than those with redshift estimates, $V = 25.4$ ($V = 24.9$), suggesting that these sources may preferentially lie at high redshift.

The last panels of Figures 5 and 6 show the IRAC colors of sources without redshift estimates. Overplotted are the star-forming contours for $z = 0 - 4$. Of the sources without redshifts, all but 1 lie inside the Lacy selection region and all but 9 lie inside the Stern selection region. This is not surprising, as sources with non-stellar continua are the hardest sources to fit. Of the 13 Lacy-selected sources, 5 lie outside the 1σ star-forming contours, and 2 have X-ray counterparts. Of the 26 PLGs, 11 lie outside the 1σ star-forming contours, and 6 are X-ray-detected. There is a noticeable concentration of X-ray non-detected PLGs towards the red end of the power-law locus. These sources are discussed in more detail in §6.